



NTNU – Trondheim
Norwegian University of
Science and Technology

Modelling of controlled wax deposition and loosening in oil and gas production systems

Oluwatosin Emmanuel Ajayi

Natural Gas Technology

Submission date: June 2013

Supervisor: Even Solbraa, EPT

Co-supervisor: Harald Kallevik, Statoil Research Center Trondheim
Knut Arild Maråk, Statoil Research Center Trondheim

Norwegian University of Science and Technology
Department of Energy and Process Engineering

EPT-M-2013-4

MASTER THESIS

for

Stud.techn. Emmanuel Oluwatosin Ajayi

Spring 2013

*Modelling of controlled wax deposition and loosening in oil and gas production systems**Modellering av kontrollert voksavsetning og- fjerning for olje og gassproduksjon***Background and objective**

A large part of worlds remaining oil and gas resources is found in harsh environments such as deep water and arctic conditions. The development of such oil and gas fields requires advanced process solutions for hydrate control, separation, dew point control and transport solutions.

Most reservoirs fluids contain heavy paraffinic components that may precipitate as a solid-like material called wax if the fluid is cooled down. Wax precipitation may cause operational problems when unprocessed well streams are transported in undersea pipelines.

During the last decade Statoil has initiated work on methods for controlled wax deposition and loosening. Such methods could potentially make possible or improve production of reservoirs with high wax content, and more particularly to enable long distance transport of oils with wax. The objective of this work will be to evaluate possible methods for controlled wax deposition and loosening (eg. heated pipelines/heat exchangers). Mechanisms of wax formation and loosening will be discussed and possible simulation tools evaluated.

The focus of this work will be on controlled wax deposition and loosening from oil dominated well streams.

The following tasks are to be considered:

1. Discussion of methods for wax deposition and loosening
2. Selection of thermodynamic model for oil-wax equilibrium
3. Development of a model for wax-precipitation and loosening
4. Use of developed model to evaluate wax deposition and loosening

-- ” --

Within 14 days of receiving the written text on the master thesis, the candidate shall submit a research plan for his project to the department.

When the thesis is evaluated, emphasis is put on processing of the results, and that they are presented in tabular and/or graphic form in a clear manner, and that they are analyzed carefully.

The thesis should be formulated as a research report with summary both in English and Norwegian, conclusion, literature references, table of contents etc. During the preparation of the text, the candidate should make an effort to produce a well-structured and easily readable report. In order to ease the evaluation of the thesis, it is important that the cross-references are correct. In the making of the report, strong emphasis should be placed on both a thorough discussion of the results and an orderly presentation.

The candidate is requested to initiate and keep close contact with his/her academic supervisor(s) throughout the working period. The candidate must follow the rules and regulations of NTNU as well as passive directions given by the Department of Energy and Process Engineering.

Risk assessment of the candidate's work shall be carried out according to the department's procedures. The risk assessment must be documented and included as part of the final report. Events related to the candidate's work adversely affecting the health, safety or security, must be documented and included as part of the final report. If the documentation on risk assessment represents a large number of pages, the full version is to be submitted electronically to the supervisor and an excerpt is included in the report.

Pursuant to "Regulations concerning the supplementary provisions to the technology study program/Master of Science" at NTNU §20, the Department reserves the permission to utilize all the results and data for teaching and research purposes as well as in future publications.


The final report is to be submitted digitally in DAIM. An executive summary of the thesis including title, student's name, supervisor's name, year, department name, and NTNU's logo and name, shall be submitted to the department as a separate pdf file. Based on an agreement with the supervisor, the final report and other material and documents may be given to the supervisor in digital format.

- Work to be done in lab (Water power lab, Fluids engineering lab, Thermal engineering lab)
 Field work

Department of Energy and Process Engineering, 14. January 2013



Olav Bolland
Department Head



Even Solbraa
Academic Supervisor

Research Advisors: Harald Kallevik and Knut Arild Maråk, both from Statoil

Abstract

A large part of worlds remaining oil and gas resources is found in harsh environments such as deep water and arctic conditions. The development of such oil and gas fields requires advanced process and transport solutions. Wax is precipitated out of solution as reservoir fluid cools down during transport. Wax precipitation may cause operational problems when unprocessed well streams are transported in undersea pipelines.

The goal of this work is to investigate modelling concept for controlled wax deposition and controlled wax loosening that is applicable to subsea flowlines in oil and gas production systems. An approach to wax control using the annulus pipe in pipe flow concept is modelled and also described.

Wax thermodynamic and deposition models is reviewed and evaluated. The review is aimed to provide accurate prediction analysis of wax precipitation and to serve as a reliable knowledge input into wax deposition modelling in oil and gas flow systems.

The cold flow concept for wax deposition solution is developed using an annulus pipe in pipe configuration for the cooling of oil below the wax appearance temperature. A wax deposition zone is created, an effect of a large temperature gradient, which is the driving force between cooling water and the flowing oil in the annulus cooling section of the pipeline. Co-current and counter current oil cooling cases is tested. The counter current annulus-cooling case is validated to adequately knock out potential wax from the oil in the wax deposition zone.

The annulus cooling approach is considered to provide an efficient and economic wax control strategy for the mechanical removal of wax in a wax control zone when pigging of wax is to be employed in a flowline eliminating excessively long pigging routes and high cost of pigging operation in typical subsea pipelines.

A wax-loosening model is further developed to determine potential loosening and potential transport tendencies of stable wax solids liberated from the wall flowline downstream the annulus.

Experimental results from the Porsgrunn flow loop of Statoil AS reveals that stable wax solid is released from wax deposits on pipeline walls when the inner wall is heated for a short period of time such that released stable wax is transported in the cool stream with no or low tendency of re-deposition downstream the flowline.

Deposited wax in the wax deposition zone is liberated using hot water sent through the annulus. Model results show re-deposition downstream the flowline. Ability of this wax deposition module to predict wax loosening is criticised. OLGA shows good representation of wax deposition growth in the annulus but incapable to represent expected wax liberation in the flowline at temperatures higher than the wax appearance temperature but below the dissolution temperature. A cold flow wax liberation model using active fluid forces with minimum wall heating for effective stripping of wax from the wax deposition zone is proposed.

Preface

This Masters thesis is written in partial fulfilment for the award of a Masters degree in Natural Gas Technology at the department of Energy and Process Engineering, Norwegian University of Science and Technology, Trondheim.

First I would like to appreciate Statoil Research and Development Centre in Trondheim for giving me the opportunity to write on this exciting concept and also providing support with the product license to the OLGA wax deposition module in the process simulator as used in this thesis work.

I also deeply appreciate my supervisor, Associate Professor Even Solbraa of the department of Energy and Process Engineering NTNU, for the guidance and qualitative feedbacks through my project and this Masters thesis. Your contributions towards the success of this work are simply invaluable and I kindly acknowledged them.

Many thanks to my co-supervisor - Knut Arild Maråk, that have initiated the terms and goals of this work, I do appreciate your insightful suggestions on how to get the work done. I also thank all Statoil colleagues that have provided help to my questions during this thesis work, Harald Kallevik, Håvard Eidsmoen, Arild Stokkenes, just to name a few. I have learnt a lot from you all.

Deep thanks goes to my father, Deac. J.A Ajayi and mother Mrs M.A Ajayi that made me live my dreams; they did provided love, help, support and prayers all thorough my studies: I could not have asked for better parents, you are loved. To my specials and siblings: Blessing, Makinde, Olumide and Precious: you are more than many in a million. I always admire you.

To all my friends from the Natural Gas Master's Programme, Overcomers International Chapel, Moholt student village - all in Trondheim, I thank you for the good times; your memories will linger on. I also appreciate David Ahanor and Aderonke Badina for taking time to proofread my texts.

Finally I thank my first baby - Omolara Damilola Daramola, for staying close, though far away - your voice kept me strong in the thin. You are so much loved.

Emmanuel Oluwatosin,

Trondheim Norway

June 2013

Table of Contents

Abstract	ii
Preface	iv
Table of Contents	v
List of Figures	vii
List of Tables	ix
Nomenclature	x
Abbreviations	14
1. INTRODUCTION	15
1.1. Wax and wax related terms.....	15
1.2. Subsea developments and wax control concepts	17
1.3. Scope of work	20
2. WAX DEPOSITION MODELS	21
2.1. Deposition Mechanisms.....	21
2.1.1. Molecular Diffusion.....	21
2.1.2. Shear Dispersion	23
2.1.3. Gravity Settling.....	24
2.1.4. Brownian diffusion	24
2.1.5. Soret diffusion.....	25
2.1.6. Shear stripping	25
2.2. Wax models	26
2.2.1. The RRR model	26
2.2.2. The Matzain model	29
2.2.3. Singh et al wax deposition model	31
3. WAX THERMODYNAMIC MODELS	35
3.1. Won Activity Coefficient Model	36

3.2.	Hansen Modified Activity Coefficient Models.....	38
3.3.	Erickson Ideal Solution Model	38
3.4.	Pedersen (1995) Wax Model	39
3.5.	Lira-Galeana et al Multi-Solid Model.....	42
3.6.	Predictive Uniquac thermodynamic model.....	44
4.	PROBLEM DESCRIPTION AND THE OLGA MODEL	49
4.1.	The OLGA wax module.....	49
4.2.	Definition of terms in PVTsim	50
4.3.	Definition of terms in OLGA.....	58
5.	RESULTS AND DISCUSSION OF CONTROLLED WAX SIMULATIONS.....	61
5.1.	Thermohydraulic simulation	61
5.2.	Base case for wax deposition simulation.....	64
5.3.	Annulus flowline cooling.....	68
5.3.1.	Co-current flowline cooling.....	71
5.3.2.	Counter current flowline cooling.....	75
5.4.	Wax Liberation Simulation.....	79
6.	A PROPOSED COLD FLOW WAX CONTROL CONCEPT.....	85
7.	CONCLUSION.....	89
8.	FURTHER WORK AND RECOMMENDATIONS.....	91
9.	REFERENCES.....	93
10.	APPENDIX.....	97
10.1.	Thermodynamics of phase fugacity and the free energy	97
10.2.	Gibbs Free Energy of pure components.....	99
10.3.	SRK expression of the fugacity coefficient	101
10.4.	Plots of wax deposition models in OLGA	102

List of Figures

Figure 1-1 Typical Direct Electric Heating configuration for subsea production system[20].....	18
Figure 1-2 Typical Direct Electrical Heating in a subsea field system[21]	18
Figure 1-3 DEH Solution on multiple pipeline segments[21]	19
Figure 4-1 Phase envelope of the oil used for wax simulations	52
Figure 4-2 Oil wax formation curve obtained from PVTsim simulation.....	57
Figure 4-3 Wax pressure-temperature curve.....	57
Figure 4-4 Profile plot of wax thickness for RRR, Matzain and Heat Analogy model after 2 days ...	59
Figure 5-1 Schematic flowline diagram.....	62
Figure 5-2 Pressure, temperature and geometry representation of the flowline	64
Figure 5-3 Base case wax deposition profile at 70 days simulation time	66
Figure 5-4 Base case wax deposition thickness with time.....	67
Figure 5-5 Overall heat transfer profile compared for wax deposition and without wax deposition ..	68
Figure 5-6 Annulus integration in the pipe line	70
Figure 5-7 Annulus combination for flowline cooling (front/end view)	70
Figure 5-8 Co-current cooling path in an annulus configuration.....	72
Figure 5-9 Wax thickness profile at the wall after annulus cooling of 70days at 500Sm ³ /day	72
Figure 5-10 Wax thickness profile at the wall after annulus cooling of 70days at 5000Sm ³ /day	74
Figure 5-11 Counter-current cooling path in an annulus configuration	75
Figure 5-12 Counter current wax thickness at the wall after annulus cooling of 70days.....	76
Figure 5-13 Counter current wax thickness after annulus cooling for 70days at increased oil rate	77
Figure 5-14 Mass balance of precipitated wax in the oil flowline after 70days simulation	78
Figure 5-15 Stabilized wax liberated from annulus in the wax deposition zone	79
Figure 5-16 Annulus combination for wax liberation.....	80
Figure 5-17 Counter-current heating path in an annulus configuration.....	80
Figure 5-18 Wax thickness profile for a counter current heating configuration after 50 days	82

Figure 5-19 Cold seeding concept in a Cold Flow Equipment[41]	84
Figure 6-1 Wax liberation concept with flow control valves	85
Figure 6-2 Annulus combination for wax liberation.....	86
Figure 6-3 Counter current heating path through an annulus flowline configuration	86
Figure 10-1 Trend plot of wax thickness in pipe 2 for RRR, Matzain and Heat Analogy model[7].	102

List of Tables

Table 3-1 Constants used to Split Pseudo component into wax and non-wax-forming parts[10].....	39
Table 3-2 Constant for Parameters A, B and C in equation (3.28).....	43
Table 4-1 Fluid Composition of oil used for PVTsim and OLGA simulation	51
Table 4-2 PT Flash Composition of oil in mole% at 1.013bar, 15°C.....	53
Table 4-3 Extended PT Flash Composition in mole% at 1.013bar, 15°C	54
Table 4-4 PT Flash Properties of Oil at 1.013bar, 15°C.....	55
Table 4-5 Wax formation data from PVTsim simulation	56
Table 5-1 Simulation cases in OLGA.....	61
Table 5-2 Oil flowline geometry.....	62
Table 5-3 Pipe material for oil flowline.....	63
Table 5-4 Input data into thermo hydraulic verification simulation	63
Table 5-5 Input data into base case wax deposition simulation.....	65
Table 5-6 Annulus flowline geometry	69
Table 5-7 Pipe Materials for Water- Annulus Flowline	71
Table 5-8 Simulation input for the annulus configuration.....	71
Table 5-9 Temperature characteristic of flowing streams	81

Nomenclature

f_i^o	Fugacity of component i
f_i^o	Standard state fugacity coefficient of component i
K_i	Equilibrium ratio
P	Pressure
R	Gas constant
T	Temperature
T_i^f	Melting temperature of component i
Z	compressibility factor
V	Molar volume
J^{sr}	Negative mass transfer due to shear force
D	Diffusion coefficient
f	friction factor
h	heat transfer coefficient
D_s	Shear dispersion coefficient
k	shear deposition rate constant
D_b	Brownian diffusion coefficient
M_b	Mass of deposited wax due to Brownian diffusion
a	Brownian particle diameter
S_f	Wetted perimeter
N_w	Number of wax components
$N_{Re,f}$	Dimensionless Reynolds number
U	Overall Heat Transfer Coefficient
r	Inner radius of pipe wall
M	Molecular weight

ΔC_p	Heat capacity
ΔH_i^f	Molar heat of fusion of component i
ΔH_i^{tr}	Molar heat of transition of component i
ΔH_i^{vap}	Molar heat of vaporisation of component i
$\frac{dC_i}{dr}$	Concentration gradient of component i
ΔC_i	Wax concentration difference between the bulk fluid and wax saturation in the oil.
C	Concentration
$\frac{dC_w}{dr}$	Concentration gradient of the wax in the bulk fluid
$\frac{dC}{dT}$	Solubility coefficient
$\frac{dT}{dr}$	Temperature gradient at the wall (radial distance) of the pipe
A	Area
d	Diameter
g	Acceleration due to gravity
k_{dep}	Thermal conductivity of wax-gel deposition
k_o	Thermal conductivity of oil phase
k_w	Thermal conductivity of wax deposition
\bar{F}	Weight fraction of solid wax in gel
G	Mass transfer rate
mfr	Mass fraction
l_{wax}	Wax thickness with time
x_i or z_i	Mole fraction of component i
$P_{c,i}$	Critical pressure

G^E	Excess Gibbs free energy
G^L	Gibbs energy in the liquid
G^f	Gibbs energy of fusion
G^{id}	Gibbs free energy of an ideal gas phase
T_i^{tr}	Transition temperature

Subscripts

i	Component of the bulk fluid in either of wax, liquid or vapour phase
w	Component of the bulk fluid in the wax phase
o	Component of the bulk fluid in the oil phase
m	Mixture components of the bulk fluid in the oil phase and the wax phase
i	Component i
L	Liquid; oil
dep	Deposition
b	Brownian diffusion

Superscripts

v	vapour
w	wax
o	oil
sr	shear force
f	fusion
vap	vapour
tr	transition
f	fusion
sh	shear force
id	ideal

Symbols

δ_i	Solubility parameter of component i
δ_w	Thickness of the wax layer
α	Thickness correction factor
ρ	Density
λ	Interaction energy
ω	Mass fraction of wax in the wax-gel layer
θ	Angle of pipe inclination
γ	Shear rate at the pipe wall
μ	Viscosity
ϕ_i	Volume fraction of component i
ϕ_w	Volume fraction of wax out of solution
ϕ	Wax porosity
τ	Shear stress
K_p	Power-law consistency index
ϕ_i	Fugacity coefficient of component i
ϕ_i^o	Fugacity coefficient of pure component i
γ_i	Activity coefficient of component i
Re	Reynolds number

Abbreviations

WAP	Wax appearance point
WAT	Wax appearance temperature equivalent to WAP
WDT	Wax dissolution temperature
WLT	Wax loosening temperature
SRK	Soave-Redlich-Kwong
PR	Peng-Robinson
EOS	Equation of state
TWS	Walls surface temperature
PVT	Pressure Volume Temperature
PVTsim	PVT simulation program
PT	Pressure Temperature
DEH	Direct Electric Heating
ASTM	American Society of Testing and Materials
Waxy fluid	Mixtures of petroleum fluid with a tendency to precipitate wax under cooling
STO	Stock tank oil
RRR	Rygg, Rydahl and Rønningsen
NTNU	Norwegian University of Science and Technology

1. Introduction

Understanding wax and wax related process has been a subject of concentrated research for the development of new solutions for deeper, colder, longer fields as well as for field developments in arctic and remote locations[1]. The viability of many of these new developments is strongly linked to proven multiphase transport strategy technologically justified at prevailing economic realities.

Wax as a flow assurance solid precipitate out of solution when the temperature of hydrocarbon fluid drops below the wax appearance temperature. Wax deposition has been studied in oil and production system and the mechanism of deposition seems fairly understood – a primary consequence of the heat and mass transfer, solubility properties of the hydrocarbon mixture and the temperature gradient between the wall of pipeline and the bulk fluid[1-3].

While recent developments aims at exploring more difficult conditions, subsea production line for multiphase-unprocessed fluids is fast becoming the benchmark for future production plans. For oil and gas productions with wax deposition tendencies; long subsea transport flowline creates a much-more deposition challenge of wax solids on the pipeline wall. A continuous wax precipitation in the bulk fluid initiates wax deposition on the walls of the flowline. Pre-planned flow assurance considerations for oil and gas field developments include detailed decision on wax control and wax remediation strategies.

Wax precipitation in oil creates an increase in the non-Newtonian behaviour of petroleum mixture and hence increased viscosity[4]. This increased viscosity reduces the flow tendencies of the fluid mixtures; It increase the cost of pumping necessary for the fluid flow[4]. Continuous wax deposition is a critical operational problem for subsea transport flowline; this may creates partial or completed pipe plugging, loss or reduced pipeline capacity, sharp pressure drop and at worst cases, wax gelling states during shutdown and restart conditions[5]. It is accounted by Granherne (2007) that wax related problems make up for about 9% of the operability issues in subsea developments[6].

1.1. Wax and wax related terms

From a chemical science point of definition, wax are mixtures of *n*-alkanes usually of the homologous chain lengths. They are hydrocarbon classes similar in composition and physical properties to beeswax from natural beehive that deform above near-ambient conditions, insoluble in water but soluble in organic, non-polar solvents[7]. Many researches have been done to determine the hydrocarbon spectrum that makes up wax composition, such include the work of Rønningsen et al.

(1991), Bishop and Philip (1994), Lira-Galeana et al. (1996) to mention a few[8]. Generally, petroleum derived wax are considered paraffinic hydrocarbons dominated by the carbon number C_{20} - C_{50} molecules, they precipitate out of solution as the fluid cools down below certain temperature threshold called the wax appearance temperature[9, 10]. Pedersen, K.S et al (2007) records that high molecular weight alkanes with higher degree of branching possess low tendencies for wax precipitation[10].

The wax appearance temperature is the temperature at which wax crystals begin to precipitate out of hydrocarbon fluids usually observed under prescribed microscopic experiments[10]. The wax appearance temperature is an important parameter used in describing and measuring wax deposition behaviour in oil and gas production. Wax precipitation temperature, wax appearance point, and wax formation temperature are familiar terms with same meaning used in many articles. It is often denoted by the acronym 'WAT'[11]. The 'WAT' acronym will in this text be used when the wax appearance temperature or the wax precipitation temperature is implied.

The cloud point is the temperature at which cloud of wax crystals is first detectable in petroleum fluid typically by the naked eye or by other typical optical detectors[12]. The cloud point serves as a useful index of the lowest temperature utility for petroleum fluid in certain applications[12, 13]. The ASTM D2500 – 11 standard test method of cloud point of petroleum mixture and the ASTM D5773 – 10 constant cooling rate method respectively describes how to determine the cloud point in petroleum mixtures[12, 13].

The pour point is regarded as the lowest temperature in which petroleum fluids lose its flow behaviour under its own weight determined by the ASTM D97, Test Method for Pour Point of Petroleum Products or the ASTM D5949 – 10, Standard Test Method for Pour Point of Petroleum Products (Automatic Pressure Pulsing Method)[10]. The pour point temperature serves as a useful determining parameter when using pour point depressant or wax inhibitor in wax precipitation and deposition management.

The wax porosity is the measure of the trapped amount of oil present in depositing wax during wax deposition[14]. It is an important index in the control of wax deposition having a direct effect on wax deposition rate. It is recorded to depend on the flow regime, flow turbulence and the type of oil[15]. Coto, B., et al (2011) discussed that porosity effects have significant influence on wax gelling in wax deposition and therefore should be included in wax thermodynamic predictive models[16]. Experimental measurement is vital to determining wax porosity of crude mixtures, as wax porosity

uncertainties still exist, importing experimental errors in wax predictions. Process simulators rely on correctly supplied wax porosity description as a vital tuning parameter for the accurate prediction of wax deposition profile in oil and gas pipelines[7].

1.2. Subsea developments and wax control concepts

In recent years, Statoil has initiated works on methods for controlled wax deposition and loosening. Previous wax control strategies have centred more on remediation options available for settling wax depositing on flowline walls and remediation options for plugged pipelines. Mechanical pigging is a widely acceptable remediation strategy designed for almost all subsea pipelines. Though widely acceptable and successful, lots of challenges attend subsea pigging which include estimating pigging frequencies, estimating wax thickness in oil pipelines before pigs are activated, risk of pig traps, variable flowline diameters, flowline geometries and host of other considerations which may result in high pigging costs or unnecessary pigging operation in oil and gas flowlines.

Chemical inhibition, active and passive temperature control are other strategies aimed at avoiding wax deposition in oil and gas flowlines[17]. Wax inhibitors and wax dispersants are the most used chemicals in wax control. Wax inhibitors in principle alter the surface structure of wax crystals thereby reducing sticking tendencies and wax growth while wax dispersant are chemicals added to precipitated wax keeping the wax dispersed in the bulk fluid[10].

Active temperature control using direct electric heating DEH or inductive heating of the flowline is a new and innovative strategy employed in few subsea flowlines[18, 19]. A typical direct electric heating configuration with power supply from a topside source is illustrated with Figure 1-1 and Figure 1-2.

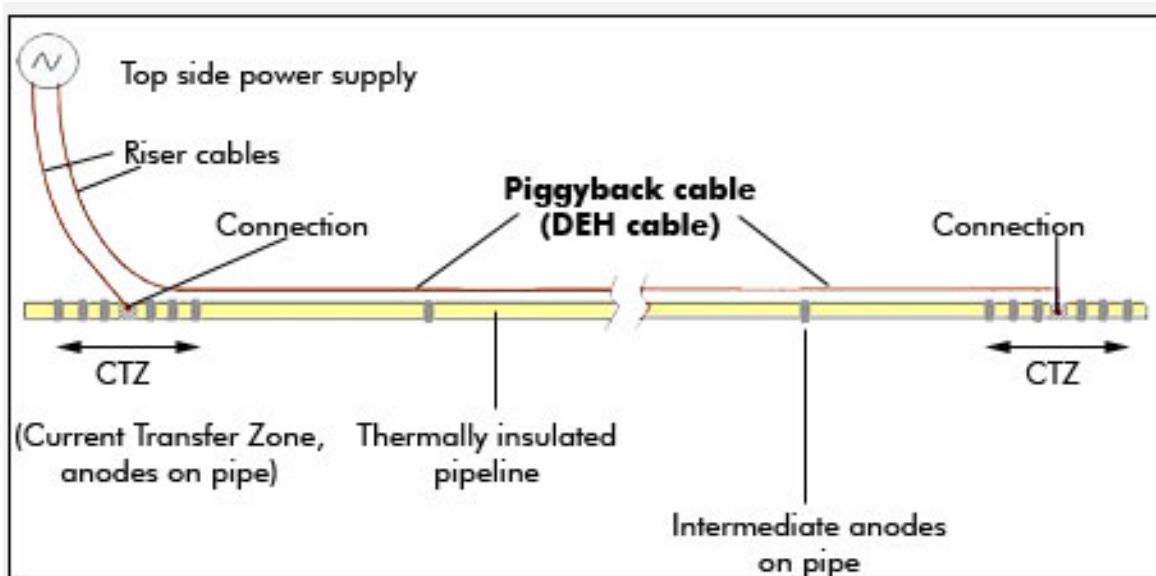


Figure 1-1 Typical Direct Electric Heating configuration for subsea production system[20]

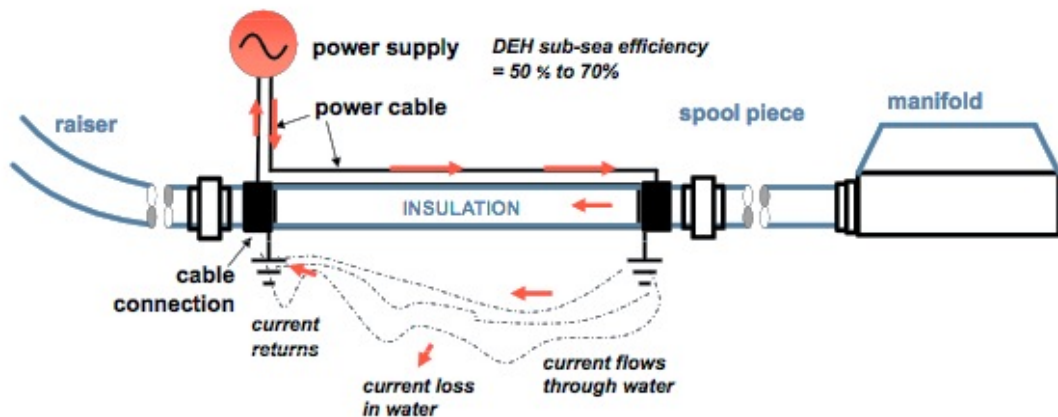


Figure 1-2 Typical Direct Electrical Heating in a subsea field system[21]

Challenges confronting the use of DEH systems include defining the accuracy of heating power needed for subsea pipeline systems, ranges and frequency of power switching in a subsea environment, temperature monitoring of a subsea flowline and installation of protective system for subsea cables. This culminates in a reduced DEH efficiency of 50% to 70% as indicated in Figure 1-2.

Creative solution proposed to the use of DEH systems includes segmentation of DEH installation on subsea pipeline such as illustrated in Figure 1-3 and the importation of power from the onshore grid.

Though novel, the success of DEH system relies on complete insulation of pipeline to avoid loss of heating energy. This comes with high cost implications and as such current implementation is limited to lengths between from 6 to 44 km per flow line on some Norwegian sea fields[20].

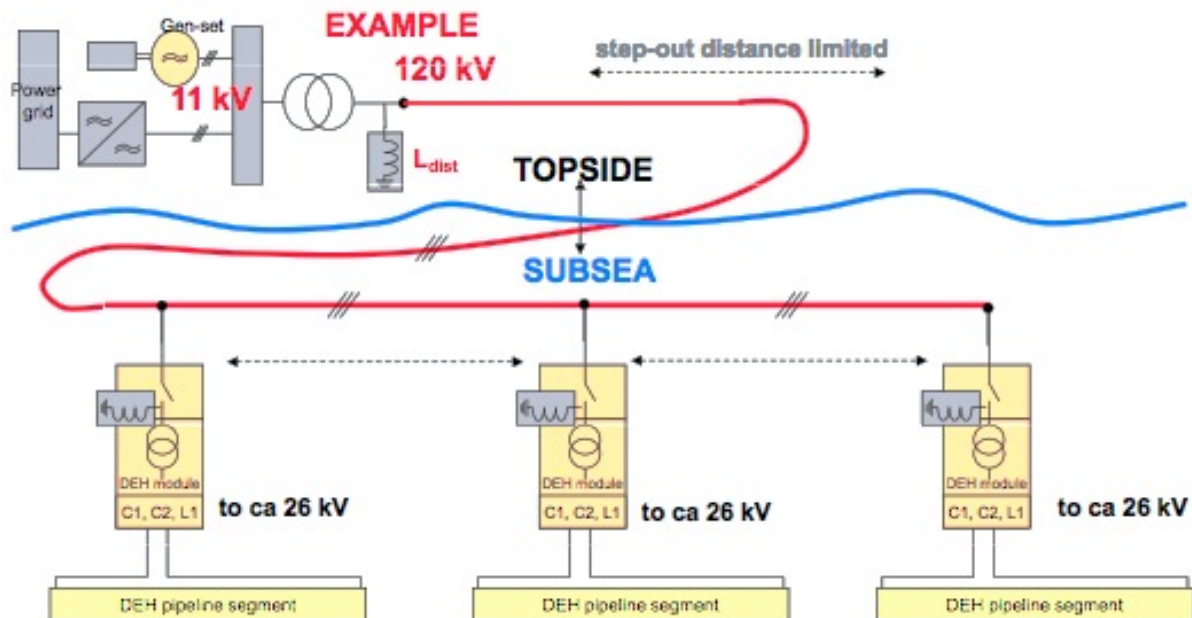


Figure 1-3 DEH Solution on multiple pipeline segments[21]

Passive temperature control includes external coating, pipe in pipe system and bundle pipelines. It is designed to maintain oil and gas temperature in the pipeline above the WAT[17]. Although chemical inhibition, active and passive temperature control presents justified control technology, applications to long subsea flowline is limited by cost and the development state of any of the chosen technology.

Cold flow concept is a new cutting-edge technology for wax control in subsea system. It operates on the mechanism of controlled slurries induced in subsea beds in subsea pipelines. It presents a new hybrid mechanism to actively manage wax and hydrates simultaneously in subsea flow lines.

Research on the cold flow has in recent time being reported to apply in producing hydrates slurries as published in the work of Turner and Talley (2008)[22]. A more recent experiment from the Statoil Porsgrunn flow loop reveals that stable wax are released when walls of subsea flowline are heated but of deep concern is the stability of wax slurries in cold flow system[19]. Solution to subsea transport challenges at present economic realities is therefore crucial.

1.3. Scope of work

Research is clearly being geared to developing new wax control technologies appropriate to new subsea initiatives. This thesis is an effort in that direction. A significant goal of this thesis is to investigate wax control modelling, evaluate the capability of process simulators in handling wax loosening models and to initiate wax deposition and loosening control model development in process simulator – such model will in principle calculate for released stable solid of wax in public process simulators. It also attempts to develop realistic cold flow approach for wax deposition and loosening in oil and gas subsea flowlines. This thesis work starts with a detailed review of wax deposition and loosening fundamental concepts in the oil and gas industry as pinpointed by the paragraphs below.

Chapter 2 of this thesis provides a review of wax models describing wax transfer between the bulk fluid and the wall surfaces. It presents how wax deposition models calculate deposition profiles and wax transport calculations implemented in investigated wax simulator codes. Chapter 3 presents an analysis of wax thermodynamic models and the thermodynamic prediction of wax precipitation in wax-oil-gas mixtures. Care is given to present difference in the thermodynamic principles so as to provide adequate understanding of precipitation analysis required for wax deposition modelling.

Chapter 4 outlines the process modelling challenges for controlled wax simulation in available process simulators as well as it investigates the underlying models implemented in the OLGA wax module. It further presents the simulation properties of the selected oil obtained through the PVTsim wax deposition package.

Results and discussion from the wax simulations carried out in OLGA is presented in Chapter 5. Deposition of wax created by co-current and counter current water-cooling in an annulus flowline provides analysis of controlled deposition in a wax control zone. Wax liberation model is simulated in OLGA and discussed. Chapter 6 examines a proposed advancement of the annulus heating of the inner wall of a pipeline with fluid stripping forces to liberated wax from the inner wall of a wax deposition zone. Chapter 7 presents the conclusion of this work while Chapter 8 entails further recommendations required for wax liberation in wax control modelling.

2. Wax Deposition Models

Wax deposition creates unwanted transport problems in oil and gas transport lines. This unwanted deposition is a major engineering challenge in the oil and gas industry[23]. For subsea transport lines over long distance, wax deposition challenges becomes very critical. As reservoir fluid leaves the wellhead, a continuous temperature decline is experienced until it reaches the temperature of the surrounding environment, which is typically below the hydrocarbon WAT. Present wax measuring technologies can easily measure or detect wax precipitation in hydrocarbon flowline but there exist some uncertainties around mechanism responsible for wax deposition. Outlined in this section are identified wax deposition mechanisms in an oil and gas process system.

2.1. Deposition Mechanisms

A couple of prior research done to evaluate wax cases have proposed different models to describe wax deposition but notable among wax depositions mechanism include Molecular diffusion, Soret diffusion, Shear stripping, Shear dispersion, Brownian diffusion and Gravity settling[1, 23, 24]. Molecular diffusion and Shear dispersion is regarded by many studies as the principal mechanisms of wax deposition. Question remains about the significance of other contributing mechanism and the impact of flow characteristic on the deposition mechanisms[14, 23]. A quick review of each of this mechanism is made to underline important wax behaviour.

2.1.1. Molecular Diffusion

Oil cooling caused by heat losses through flowline walls creates radial temperature gradients between the inner wall of the flowline and the boundary layer of the flowing fluid. The experiment of Burger et al (1981) explains that a thin laminar sublayer exist between fluids in pipeline and the pipe wall[25]. Temperature gradient across the laminar sublayer creates wax precipitation when oil cools below the WAT. This temperature gradient around the pipe walls creates a concentration gradient of dissolved wax subsequently transported to the pipe wall by a diffusion process[25, 26]. Precipitation of wax occurs at contacts between dissolved wax solution and the cool wall surface[25]. The experiment of Burger et al (1981) confirms that molecular diffusion dominates as the primary mechanism at high temperature heat flux condition typical of subsea flowline systems[25]. He showed that the Fick's law of diffusion could model molecular diffusion of solid wax in oil and gas flows.

$$\frac{dM_w}{dt} = \rho_w D_w A_w \frac{dC}{dr} = \rho_w D_w A_w \frac{dC}{dT} \frac{dT}{dr} \quad (2.1)$$

Where $\frac{dM_w}{dt}$ is the rate of wax deposited (kg/s), ρ_w is the density of the solid wax (kg/m³), D_w is the diffusion coefficient of the wax in the oil phase (m²/s), A_w is the area of wax deposition (m²), $\frac{dC}{dr}$ is the wax concentration gradient (1/m) of wax concentration over pipe radial coordinate r (m), $\frac{dC}{dT}$ is the solubility coefficient of the wax crystal in the oil phase (1/°C), $\frac{dT}{dr}$ is the radial temperature gradient of the wall (°C/m).

Burger et al. (1981) proposed the experimental correlation of Wilke Chang (1955) for the diffusion coefficient where T_a is the absolute temperature (Kelvin), M is the molecular weight of the oil solvent (g/mol), V is the wax molar volume (cc./g.mole), μ is the dynamic viscosity (cP) and ξ is a association parameter representing the effective molecular weight of the solvent with respect to molecular diffusion.

$$D_w = 7.4 \times 10^{-9} \frac{T_a (\xi M)^{0.5}}{\mu V^{0.6}} \quad (2.2)$$

Given that $V^{0.6}$ is proportional to the absolute temperature T_a . The association parameter ξ and the molecular weight of the oil solvent M are constants in the equation. The diffusion coefficient in principle is proposed as a function of oil constant C_1 and oil viscosity in many diffusion coefficient models[25, 26] as given by equation (2.3). The C_1 constant has been primarily used as tuning parameter in many wax models and in wax deposition simulators to tune diffusion coefficient to fitting experimental values.

$$D_w = \frac{C_1}{\mu} \quad (2.3)$$

Lindeloff and Krejbjerg (2002) accounts that Hayduk And Minhas (1982) correlation developed for n -paraffin can also be used to determine the diffusion coefficient as expressed in equation (2.4), given that T is the temperature (Kelvin), μ is the dynamic viscosity (cP), V is the molar volume in cm³/g[11].

$$D_m = 13.3 \times 10^{-12} \times T^{1.47} \frac{\mu \left(\frac{10.2}{V} \right)^{-0.791}}{V^{0.791}} \quad (2.4)$$

Where $V = \frac{M}{\rho_w}$.

The Hayduk and Minhas (1982) correlation is implemented in PVTsim DepoWax module to calculate the deposition rate by molecular diffusion but integral to the PVTsim model is a supplied associated tuning coefficient that allows for user tuning possibility when it is essential to tune to experimental data in order to account for unrealistic low or high deviation in diffusion coefficient.

2.1.2. Shear Dispersion

Shear dispersion as a mechanism of wax deposition is observed when already precipitated wax particles flowing at mean speed of a bulk fluid is acted on by wall forces and intermolecular forces of the flowing stream[11, 25]. A shear field exist where slower moving particles interact with nearby-faster moving particles at the centre of streamlines in a fluid flow. For high concentration of wax particles, these wax particle interaction creates large temporary displacement generating a net lateral transport of wax on flowline walls[25]. Burger et al conducted experimental work at low temperature heat flux condition where deposition by molecular diffusion is expected to be zero, his experiment produced little or no measurable wax deposition and he concludes that shear dispersion only becomes relevant in low temperature and low heat flux conditions although the University of Tulsa wax experiment and the Statoil Porsgrunn flow loop wax experiments have both indicated an insignificant shear dispersion deposition[11, 25]. Assumptions on shear dispersion still remains with suggestion that wax dispersion exist as a wax removal mechanism by some researchers[26].

Shear dispersion can be modelled by the dispersion coefficient of Burger et al (1981) given in equation (2.5) where γ_o is the oil shear rate at the pipe wall (s^{-1}), d_w is the wax particle diameter (m), ϕ_w is the wax volume fraction out of the solution at the wall and D_s is the shear dispersion coefficient (m^2/s).

$$D_s = \gamma_o \frac{d_w^2 \phi_w}{10} \quad (2.5)$$

2.1.3. Gravity Settling

Density effects on wax crystal as compared to its surrounding oil solvent presents a potential gravity deposition mechanism in non-interacting oil-wax systems. Burger et al (1981) accounts settling effect in gravity fields due to wax settling velocity[25]. This velocity diminishes asymptotically to zero as wax-oil fluid reaches complete settling. In typically active system as found in oil and gas pipelines, gravity settling have been found to be negligible as suggested shear dispersion mechanism or active fluid forces create dispersion of precipitated wax particles eliminating gravity settling[25, 26]. However in low flow rates, at typical shut in conditions or in storage tanks, gravity effect is expected to contribute to significant wax deposition particularly observed for low viscous fluids[17]. The settling velocity U (m/s) is given by the modified stokes law of settling crystals in a pseudoplastic fluid[17].

$$U = \left[\frac{g \Delta P a^{(1+n)}}{18 K_p} \right]^{1/n} \quad (2.6)$$

Where ΔP is the density difference (kg/m^3) between the settling wax and the oil, a the particle diameter (m), n the power-law index, g the acceleration due to gravity (m/s^2) and K_p is the power-law consistency index.

The shear rate and shear stress relationship of a power law fluid implied in the correlation is given to be $\tau = K_p \gamma^n$ where τ is the shear stress (N/m^2) and γ is the shear rate of the fluid (s^{-1})[17].

2.1.4. Brownian diffusion

Agitated oil molecules bombard precipitated wax suspended in waxy-oil flows. This creates net irregular movement of wax particles[25]. If concentration gradients exist for the wax solid, a net transport of the precipitated molecules is initiated in the direction of decreasing concentration modelled by the Fick's law of diffusion in equation (2.7)[26].

$$\frac{dM_B}{dt} = \rho_w D_B A_w \frac{dC}{dr} \quad (2.7)$$

Where M_B is the mass of deposited wax due to Brownian diffusion (kg), $\frac{dC}{dr}$ is the concentration gradient over the pipe radial coordinate (1/m), A_w is the area of wax deposition (m^2) and D_B the Brownian diffusion coefficient (m^2/s) derived by equation (2.8).

$$D_B = \frac{RT_a}{6\pi\mu aN} \quad (2.8)$$

And R is the gas constant (J/(mol·K)), T_a is the absolute temperature (K), μ is the oil viscosity (Ns/ m^2), a is the Brownian particle diameter (m) and N is Avogadro's number (mol^{-1}).

A number of contributing researches such as from the work of Burger et al (1981), Rosvold (2008), Singh et al (1999) considers no significant influence of Brownian diffusion but Azevedo and Teixeira (2003) believes there are no experimental evidence to justify this conclusion[11, 25, 26].

2.1.5. Soret diffusion

Mass transfer between the bulk fluid and the inner wall of the pipeline due to thermal diffusion is called Soret diffusion or the Soret Effect[26]. Soret diffusion is modelled by the Fick's diffusion equation with a Soret coefficient. Although some authors have categorized thermal diffusion to be negligible, it is comprehensive to represents diffusion terms by all possible diffusion effect that could potentially influence wax deposition in wax deposition modelling[26].

2.1.6. Shear stripping

Shear stripping or shear sloughing or shear removal is the mechanism of wax removal from the walls due to shear stress exerted by flowing stream of oil on the wax solid. The inflowing velocity can sloughs pieces of wax from the deposition layer thereby acting as a wax removal mechanism. Shear stripping is observed if concentration gradient develops between the wax on the walls and sloughed waxes in the bulk fluid[24].

The negative wax transfer due to shear forces is modelled as a function of the shear stress τ , thickness of the wax layer δ (m), and the wax layer yield stress. It is recorded by Pan et al (2009) that

the wax yield stress is proportional to $\omega^{2.3}$ such that ω is the mass fraction of wax in gel layer[24]. The wax shearing rate is derived based on the Edmonds et al (2007) shear rate equation of (2.9)[23].

$$J^{sr} = c \frac{\delta \tau}{\omega^{2.3}} \quad (2.9)$$

Where c is the shear constant, ω is the mass fraction of wax in gel layer, δ (m) is the thickness of the wax layer, τ is the shear stress (N/m²) is as obtained by the equation (2.10) such that f is the fanning friction factor ρ_o is the density of the flowing oil (kg/m³) and u_o is the oil velocity (m/s).

$$\tau = \frac{1}{2} f \rho_o u_o^2 \quad (2.10)$$

The University of Tulsa deposition experiments records higher wax deposition thickness in laminar flow than in turbulent flow, an observation attributed to the effect of shearing force acting as a limiting mechanism in the deposition experiment in turbulent flow [27]. It further accounted that in turbulent flows, shear stress exerted by the fluid flow on the depositions creates a rapid transport of deposited or dissolved wax which may be sufficiently high to mechanically remove some of the formed wax deposits from the walls[25].

2.2. Wax models

2.2.1. The RRR model

The RRR (Rygg, Rydahl and Rønningsen) wax model is a multi phase wax model used in predicting wax deposition properties in pipelines and oil and gas systems. The RRR model implements molecular diffusion and shear dispersion effect as the mechanisms responsible for wax deposition[11]. It performs a continuous estimate of the wax build-up along the pipeline over integrations of time for a multicomponent mixture. The RRR steady state flow model calculates flow properties using integrated wax-PH flash properties for the composition in the oil –wax rich stream. It is considered a steady state model because the wax deposition time takes a much longer time when compared with to active flow process and system disturbances time in a typical oil and gas pipeline[28].

The RRR model functions as a integrator of sub models that account for the pressure drop and regime changes, viscosity of the fluid mixture, heat and energy balances, wax thermodynamic properties and wax transport mechanism itself[11, 28]. It is a fully compositional model as it accounts for an

individual representation of the property of components in the sub-model while keeping track of each compositional behaviour using heat, mass and energy balances on discretized sections of the pipeline[11].

The total volume rate of deposited wax given as l_{wax} is calculated as a sum of two contributing mechanism namely molecular diffusion and shear dispersion as calculated by equation (2.11) such that ϕ is the wax porosity with values in the range of 0.6-0.9.

$$l_{wax} = \frac{Vol_{wax}^{diff} + Vol_{wax}^{shear}}{(1-\phi)2\pi rL} \quad (2.11)$$

The wax porosity - an important wax property represents the amount of oil trapped within the wax pore spaces[28]. It is implemented as a useful tuning parameter of the wax oil calculation in OLGA and PVTsim wax simulation code. It further used as an index of the shear effect and wax roughness effect on the walls of the pipeline which is important in accounting for pressure drop and gelling in non-flowing wax-oil systems.

The volume rate of wax deposited by molecular diffusion imputed into the RRR model for each wax-forming component i is obtained from equation (2.12)[28]. Hayduk and Minhas correlation is used to calculate the wax diffusion coefficient D_i for component i in the wax phase.

$$Vol_{wax}^{diff} = \sum_{i=1}^{N_w} \frac{D_i (\Delta C_i) S_f M_i}{\delta \rho_w} 2\pi rL \quad (2.12)$$

Where N_w is the number of wax component, D_i is the diffusion coefficient (m^2/s), ΔC_i is the concentration difference between the bulk phase and the wax phase for component i , S_f is the fraction of wetted perimeter by wax, M_i is the molecular weight (g/mol), L is the length of the pipe (m), r is the effective inner pipeline radius to account for wax deposition (m), ρ_w is the density of wax component i (kg/m^3) and δ is the thickness of the laminar sub layer (m).

The thickness of the laminar sub layer in the pipeline is obtained by the Bendiksen et al. (1991) correlation in equation (2.13) such the α is a allowed correction factor for tuning thickness of the wax layer to experimental data[28].

$$\delta = \alpha \times 11.6 \sqrt{2} \frac{D}{Re} \frac{1}{\sqrt{f}} \quad (2.13)$$

Given that D is the pipe diameter (m), Re is the Reynolds number and f is the friction factor. The Blasius equation is used to calculate the thickness of the sub-layer in turbulent flows[11].

The shear dispersion contribution in the volume of wax deposited is derived by the modified Burger et al. (1981) equation in (2.14) where k is the shear deposition constant, ϕ_w is the volume fraction of deposited wax in the bulk fluid, γ is the shear rate in the oil (s^{-1}), ρ_w is the average density of wax precipitated in the bulk fluid (kg/m^3) and A is the surface area available for deposition (m^2)[11, 29].

$$Vol_{wax}^{shear} = \frac{k\gamma A\phi_w}{\rho_w} \quad (2.14)$$

It is noteworthy to mention that the magnitude of shear dispersion contribution is nearly negligible when compared to the molecular diffusion; therefore shear coefficient constant in the order of $(0;0.0001)g/cm^3$ or $(0;0.001)kg/m^2$ is supplied into the model to account for the small shear dispersion corresponding magnitude[28].

Further questions arises for the non-implementation of other contributing wax deposition mechanism and more significantly, the non-inclusion of the shear stripping mechanism to account for shear removal of wax in high velocity flows and the how the RRR model justifies flow regime changes.

Nevertheless, experimental results from the work of Rygg et al. (1998) for predicting the wax-build up, temperature and pressure calculation with time has shown good and consistent agreement between calculated and observed pressure losses for single and multiphase pipe systems[11].

Implemented in the RRR model is a dissolution model of wax from the wall. It is calculated as a function of the concentration derivative of the wax with respect to temperature change between the bulk fluid and the wall. The dissolved wax concentration found at the cloud point for each pressure section is calculated as follows

$$C_{W,wall} = C_{W,TWS} + \left. \frac{dC_{wax}}{dT} \right|_{WAT} (TWS - WDT) \quad (2.15)$$

Where $C_{W,wall}$ is the concentration of the wax at the wall obtained from the normal diffusion equation, $C_{W,TWS}$ the concentration of wax adjusted to account for increase in wall temperature, TWS the wall surface temperature, WDT the wax dissolution temperature, WAT the wax dissolution temperature and $\left. \frac{dC_{wax}}{dT} \right|_{WAT}$ the concentration derivative with respect to temperature at the cloud point.

The wax dissolution temperature is obtained as the sum of the wax appearance temperature and the dissolution difference $\Delta T_{dissolution}$ given in equation (2.16).

$$WDT = WAT + \Delta T_{dissolution} \quad (2.16)$$

As rightly pointed out, concentration gradient existing between the bulk fluid and wax wall $C_{W,bulk} - C_{W,wall}$ drives the diffusion process. For a wax melting process, the concentration difference condition must be present such the concentration of wax at the wall is greater than the precipitated wax in the bulk fluid: $C_{W,wall} > C_{W,bulk}$ [29].

The dissolution model in the RRR provides an advantage over other wax deposition model when wax removal or wax loosening modelling is to be considered in active deposition systems.

2.2.2. The Matzain model

The Matzain model incorporates shear stripping alongside molecular diffusion and shear dispersion as potential wax deposition models. The shear stripping model serves as a wax reducing mechanism in the Matzain implemented model. A Fick's law modification by Matzain et al (2001) accounts for the stripping contribution in the model. The rate of wax build up in a wax deposition process is obtained by equation (2.17)[27].

Where $\frac{d\delta}{dt}$ is the change in wax thickness deposited on the wall layers with time (m/s), D_{ow} the diffusion coefficient obtained from the Wilke and Chang correlation in equation (2.2), C_w the concentration of wax in solution (weight %), r the pipe radial distance (m) and T the bulk fluid temperature (C).

$$\frac{d\delta}{dt} = \frac{\Pi_1}{1 + \Pi_2} D_w \left[\frac{dC_w}{dT} \frac{dT}{dr} \right] \quad (2.17)$$

Supplied empirical correlations for Π_1 accounts for porosity effect on rate of wax deposited. It as well accounts for other deposition enhancement mechanism not accounted by diffusion coefficient. Π_2 accounts for wax limiting effect of shear striping[27, 28].

$$\Pi_1 = \frac{C_1}{1 - C_L / 100} \quad (2.18)$$

The porosity effect coefficient C_L in equation (2.19) defines the amount of oil trapped in the wax layer. A regime dependent Reynolds number in a multiphase flow system calculates for flow regime changes. The Matzain constant in equation (2.18) $C_1 = 15$.

$$C_L = 100 \left(1 - \frac{N_{Re,f}^{0.15}}{8} \right) \quad (2.19)$$

The dimensionless parameter $N_{Re,f}$ is obtained as a function of the effective inside diameter of the pipeline after taking wax build-up into account.

$$N_{Re,f} = \frac{\rho_L v_L d_w}{\mu_L} \quad (2.20)$$

The shear stripping effect is calculated by equation (2.21) with the Matzain constants $C_2 = 0.055$ and $C_3 = 1.4$ respectively.

$$\Pi_2 = 1 + C_2 N_{SR}^{C_3} \quad (2.21)$$

It is observed that the Matzain constants C_1 , C_2 and C_3 have been supplied as flow parameters accounting for single phase and two-phase flows behaviour in this correlation.

The flow regime dependent Reynolds number N_{SR} is calculated for each regime by equation (2.22), (2.23) and (2.24) where ρ_L is the oil density (kg/m^3), v_L the oil velocity (m/s), δ the wax layer thickness (m) and μ_L the viscosity of the oil ($\text{kg/m}\cdot\text{s}$)[28].

This incorporated regime correlations explicitly suggest that potential higher accuracy could be obtained from the Matzain model relative to the RRR model. The wax model predictions result for the implemented OLGA models compared in the work of Ajayi E.O (2013) confirms a higher prediction accuracy of the Matzain model[7]. This stresses a need for flow regime correlations and the importance of mixture velocity input in the wax predictions.

The implemented flow regime Reynolds number in the Matzain model is given by equations (2.22), (2.23) and (2.24)[29].

$$\text{Single phase and stratified wavy flows} \quad N_{SR} = \frac{\rho_L v_L \delta}{\mu_L} \quad (2.22)$$

$$\text{Bubble and Slug flow} \quad N_{SR} = \frac{\rho_m v_L \delta}{\mu_L} \quad (2.23)$$

$$\text{Annular flow} \quad N_{SR} = \frac{\sqrt{\rho_m \rho_L} v_L \delta}{\mu_L} \quad (2.24)$$

The thermal gradient of the laminar sub layer for the deposition is found by equation (2.25)[11].

$$\frac{dT}{dr} = \frac{(T_b - T_{wall})}{k_L} h_{wall} \quad (2.25)$$

Where k_L is thermal conductivity of the oil (W/mK), h_{wall} the inner wall heat transfer coefficient (W/m²K), T_b is bulk fluid temperature (K) and T_{wall} the inner wall surface temperature (K).

2.2.3. Singh et al wax deposition model

Singh et al (2000) presented another wax model development using the thin-film concept. Underlining modelling principle in the thin film concept rest on the University of Michigan deposition experiments where particulate deposition is studied in wax layer. Singh et al (2000) opined that a non-uniform diffusion occurs in wax deposits as a result of a concentration gradient existing in the sub layer of wax deposits. It considers an internal diffusion mechanism for waxy gel layers inducing physical gelation on the wall[30].

The initial formation of wax at the wall serves as the beginning of the deposition process while trapped oil between successive wax layers provide opportunity for further internal diffusion for

continued wax deposition. An incipient wax, gels in the 3-D network structure of the wax such that strong physical affinity between wax layer and incipient wax is produced[30].

The thin film wax therefore gels with cooling. Gelation rate depends on cooling rate between waxy oil and pipe walls. The wax molecules diffuse to form wax deposits as a result of n -existing concentration gradient between diffusing wax molecules and the wax deposition surface, which creates a non-uniform hardening in the pipe radial direction. This confirms the porous characteristics of wax layers. The increase in the wax fraction in the wax deposit with time is called ageing of wax[31]. The Singh et al model further considers a counter diffusion process of oil molecules out of wax deposit in wax layers[31].

Wax deposition prediction is implemented through the coupling of the thin film approach with heat and mass balances to calculate thickness and radial composition in pipelines. The heat mass balances is obtained from a combination of couple partial differential and algebraic equations found in the work of Singh et al (2001)[31].

The material balance for the growth of wax thickness is presented below.

$$\frac{d\delta}{dt} = \frac{D_{ow} \left. \frac{dC}{dr} \right|_i [1 - \phi(x)]}{\rho x} \quad (2.26)$$

$$\frac{dx}{dt} = \frac{D_{ow} \left. \frac{dC}{dr} \right|_i \phi(x) 2(R - \delta)}{\rho \delta (2R - \delta)} \quad (2.27)$$

Where δ is the deposit thickness (m), x the wax content in the deposit, R the radius of the clean pipe (m), D_{ow} the diffusion coefficient of the wax in oil (m^2/s) and ϕ the porosity factor found by Cussler as equation (2.28)[11].

$$\phi(x) = \frac{1}{1 + \alpha \left(\frac{x^2}{1 - x^2} \right)} \quad (2.28)$$

Given that α is the aspect ratio of the wax crystal. The value of the aspect ratio starts at 1 and increases with reducing oil fraction in the deposit.

This approach to wax modelling is credited as the only model found to implement aging and gellation of wax into its deposition prediction. It clearly demonstrates that the wax content of depositing wax in a deposition process varies across wax layers in diffusion as against other wax model predictions.

Furthermore, the ageing of precipitated wax depends on the wax oil operating condition; a strong function of the flow parameters namely the flow velocity and wall temperature. The wax gel concentration on the wall therefore changes as a function of depleted wax concentration in the bulk fluid and the wax layers.

Field data verification of Singh, A. et al (2011) recorded higher deposition rate than other equilibrium model for wax prediction[32]. A setback to this model is its limitation to thin films and therefore unsuitable for thick gelling deposition and its need for modification in turbulent flows[31, 32].

3. Wax Thermodynamic Models

Accurate thermodynamic description is fundamental to the prediction of wax deposition in hydrocarbon mixtures. For estimating deposition kinetics, underlining thermodynamic equilibrium relations must be understood and accurate, unclear understanding of equilibrium thermodynamics produces inaccurate deposition calculations. Approaches made to model thermodynamics of wax include the solution theory modelling approach of Won (1986 and 1989), the oil-wax equilibria work of Hansen et al (1988) and Erickson et al (1993), the multi solid wax solution precipitation of Lira-Galeana et al (1996), the Uniquac model of Coutinho (2006) and the vapour–liquid–solid equilibrium model using the activity coefficient approach of Pedersen, K.S et al (2007). Each of theses thermodynamic models presents different degrees of uncertainties[8, 10]. A careful and a quick review of these models are presented below to provide the thermodynamic selection for precipitation, deposition and control models investigated in this thesis.

Generally, wax precipitation description models rely on principles that calculates oil-wax equilibrium parameters and thermo physical prediction that relates thermo-physical properties of n -paraffin in wax solutions with the thermo-physical properties of its pure components at standard condition[33].

Equilibrium modelling of wax-oil-gas phases depend on the equality of phase fugacity of each phase present in a multi-phase system[34]. The wax phase is a solid phase. The solid phase and the wax phase are terms used interchangeably to mean the wax phase and vice versa in many wax thermodynamic models description. In this thesis the wax-solid phase is described by the subscript W , the liquid phase (oil) with subscript L and the gas phase (vapour) V respectively.

At equilibrium, phase fugacity equality is achieved such that the equality of fugacity is given by equation (3.1) where f_i^W is the wax fugacity of component i in the solid phase, f_i^L the oil fugacity of component i in the liquid phase and f_i^V the gas fugacity of component i in the gas phase respectively[10].

$$f_i^W = f_i^L = f_i^V \quad (3.1)$$

Pedersen, K.S et al (2007) commented that differentiating difference in available wax thermodynamics models centres on the different models describing the phase fugacity[10]. Pedersen went on to define the fugacity of oil and the wax phase as a product of mole fraction, activity coefficient and the phase fugacity of pure component where x_i is the mole fraction of component i , γ_i

the activity coefficient of component i and f_i^o the fugacity of pure component i at the same temperature and pressure in the wax and oil phases respectively[10].

Such that the wax fugacity
$$f_i^W = x_i^W \gamma_i^W f_i^{oW} \quad (3.2)$$

and the oil fugacity
$$f_i^L = x_i^L \gamma_i^L f_i^{oL} \quad (3.3)$$

3.1. Won Activity Coefficient Model

Won's activity coefficient model utilizes the regular solution theory to characterize all hydrocarbons components. He argued that all hydrocarbon components possess crystal stable ability and as such potential wax formers assigned with n -paraffin solubility parameters[33].

Won activity coefficient is defined by the solubility parameter $\bar{\delta}$ ($\text{cal}/\text{cm}^3)^{0.5}$, the volume fraction Φ_i of components i and the molar volume V_i (cm^3/mol) of components i present in the hydrocarbon mixture. Equation (3.4) gives the solid and the liquid phase activity coefficient where R is the gas constant ($\text{cal}/(\text{mol}\cdot\text{K})$).

$$\ln \gamma_i^W = \frac{V_i^W (\bar{\delta} - \delta_i^W)^2}{RT}; \quad \ln \gamma_i^L = \frac{V_i^L (\bar{\delta} - \delta_i^L)^2}{RT} \quad (3.4)$$

The solubility parameter in the wax and the oil phase is defined through sets of equilibrium parameters of individual components present in solution by equation (3.5).

$$\delta_i^W = \sqrt{\frac{\Delta H_i^{\text{vap}} - \Delta H_i^f - RT}{V_i^S}}; \quad \delta_i^L = \sqrt{\frac{\Delta H_i^{\text{vap}} - RT}{V_i^L}} \quad (3.5)$$

Where ΔH_i^{vap} is the molar heat of vaporization (cal/mol), ΔH_i^f the enthalpy of fusion (cal/mol), T the temperature (K) and V_i the molar volume of components i present in solution.

Won expression for melting enthalpy ΔH_i^f and for melting temperature ΔT_i^f is given by equation(3.6) [10].

$$\Delta H_i^f = 0.1426M_i T_i^f; T_i^f = 374.5 + 0.0261M_i - \frac{20172}{M_i} \quad (3.6)$$

The solubility property $\bar{\delta}$ defined by the volume fraction Φ_i of component i in the wax and oil phase is given in equation (3.7). The volume fraction Φ_i is further derived as a function of the molar volume and the mole ratio of component i in solution in both phases as given by equation (3.8).

$$\bar{\delta}^W = \sum_{i=1}^N \Phi_i^W \delta_i^W; \bar{\delta}^L = \sum_{i=1}^N \Phi_i^L \delta_i^L \quad (3.7)$$

$$\Phi_i^W = \frac{x_i^W V_i^W}{\sum_{j=1}^N x_j^W V_j^W}; \Phi_i^L = \frac{x_i^L V_i^L}{\sum_{j=1}^N x_j^L V_j^L} \quad (3.8)$$

Won showed that the molar volume for the solid and liquid phase is obtained by equation (3.9) where M_i is the molecular weight (g/mol) and $d_{i,25}^L$ is the liquid density (g/cm³) of component i at 25°C - equation (3.10)[10].

$$V_i^W = V_i^L = \frac{M_i}{d_{i,25}^L} \quad (3.9)$$

$$d_{i,25}^L = 0.8155 + 0.6273 \times 10^{-4} M_i - \frac{13.06}{M_i} \quad (3.10)$$

Pedersen et al (2007) records that the wax-oil equilibrium definition of Won (1986) is further derived to give wax fugacity from the fugacity term of pure component i in the liquid phase as recorded by equation (3.11) but he neglected the heat capacity and pressure term of phase transitions[10, 35].

$$f_i^W = x_i^W \gamma_i^W f_i^{oL} \exp\left(-\frac{\Delta H_i^f}{RT} \left(1 - \frac{T}{T_i^f}\right)\right) \quad (3.11)$$

Further work of won in 1989 records a higher heat capacity influence on the solubility of nC_{36} in nC_{12} than on the heat capacity influence of nC_{28} in nC_5 . This motivated the modification of the solid phase fugacity to include the heat capacity term as defined in equation (3.12) where ΔC_p is the heat capacity change between phases[10, 35].

$$f_i^W = x_i^W \gamma_i^W f_i^{oL} \exp\left(-\frac{\Delta H_i^f}{RT}\left(1-\frac{T}{T_i^f}\right) - \frac{\Delta C_p}{R}\left(1-\frac{T_i^f}{T} + \ln\frac{T_i^f}{T}\right)\right) \quad (3.12)$$

At equilibrium, equation (3.1), (3.3) and (3.12) is combined to give equation (3.13). This is used to calculate activity coefficient of large molecules in lower molecular weight oil solvents which is also applied for activity coefficient of oil-wax mixtures[10, 35]. Activity coefficient of Won is obtained in the order of 0.7 and 1.0[10].

$$\frac{x_i^L}{x_i^W} = \frac{\gamma_i^W}{\gamma_i^L} \exp\left(-\frac{\Delta H_i^f}{RT}\left(1-\frac{T}{T_i^f}\right) - \frac{\Delta C_p}{R}\left(1-\frac{T_i^f}{T} + \ln\frac{T_i^f}{T}\right)\right) \quad (3.13)$$

The generalisation of hydrocarbons in the fluid mixture as potential wax formers and the limitation of the Won's model to solid liquid equilibrium have made it inappropriate for gas rich mixtures. The coupling of two models namely a wax-oil activity coefficient model and another liquid-gas model such as a cubic EOS model creates thermodynamic inconsistencies and alters the equilibrium criteria for solid-liquid-vapour equilibrium in thermodynamic systems.

3.2. Hansen Modified Activity Coefficient Models

Hansen et al (1988) used the generalized polymer solution theory to modify the liquid phase activity coefficient. He presented modified activity coefficient of the solid phase by formulating thermodynamic relationship between the viscosity term and the surface tension[36]. Hansen presented a modification of the liquid phase fugacity and the solid phase fugacity to rectify high WAT inconsistencies in his stabilized oil mixtures. The modified activity model considers the wax phase as an ideal mixture with an activity coefficient of unity and the liquid phase activity coefficient of the order of 10^{-10} [10].

3.3. Erickson Ideal Solution Model

Erickson et al (1993) accounts the need to differentiate potential wax forming component and non-wax forming component based on the premise that *iso*-paraffin with lower melting and boiling point has a reducing effect on the WAT than *n*-paraffin[10]. It distinguishes wax and non-wax forming components by assuming ideal solution of pure components in the liquid and solid phases thereby neglecting the activity coefficient.

The model is justified through exponential influence of the heat of fusion ΔH_i^f on the solid-state fugacity term from equation (3.5). Experimental observation records by Pedersen et al (2007) noted that not all components of stable oil dominated by C₁₀₊ fractions is converted into solid wax when cooled below the melting temperatures further confirming the presence of non-wax forming components unlikely to take part in wax formation[10].

3.4. Pedersen (1995) Wax Model

Pedersen et al (2007) records the advancement of Erickson ideal solution hypothesis as modified by Rønningsen et al (2007) that only *n*-paraffin with C₇₊ fraction can form and contribute to wax formation[10]. He defined a relationship for wax-forming fraction by a wax mole fraction z_i^W , which is given as a function of the density and the molecular weight M_i in equation (3.14) such that z_i^{tot} is the total mole fraction of carbon number fraction *i*, ρ_i the average density and ρ_i^P the density of normal paraffin with same molecular weight as the carbon number fraction *i*[10].

$$z_i^W = z_i^{tot} \left[1 - (A + B \times M_i) \left(\frac{\rho_i - \rho_i^P}{\rho_i^P} \right)^C \right] \tag{3.14}$$

Where A, B and C are constants given in Table 3-1.

Table 3-1 Constants used to Split Pseudo component into wax and non-wax-forming parts[10]

A	1.074
B	6.584 x 10 ⁻⁴
C	0.191

The density of normal paraffin ρ_i^P (*wax forming paraffin*) with same molecular weight as carbon number with fraction *i* as obtained from equation (3.15).

$$\rho_i^P = 0.3915 + 0.0675 \ln M_i \tag{3.15}$$

The mole fraction of non-wax forming part in a mixture calculated by equation (3.16) is obtained as the difference between the total mole fraction and the mole fraction of the wax forming part in the mixture[10].

$$z_i^{nonwax} = z_i^{tot} - z_i^W \quad (3.16)$$

Implications of the Pedersen constants in Table 3-1 predict that wax-forming fraction decreases with molecular weight. This is consistent with the assumptions that n -paraffin forming parts decreases with carbon number[10]. Aromatic hydrocarbon with higher density terms for the carbon number creates a reducing wax content by equation (3.14). The density term clearly provide characteristic information of oil fractions with respects to paraffinic content. A negative wax-forming fraction is taking as zero as recorded in Pedersen et al (2007)[10].

Based on the model of Erickson, the ideal solution fugacity of the wax phase is given as equation (3.17). Detailed description on how to calculated the pure component fugacity of the solid wax of equation (3.18) at pressure P is obtained in Appendix 10.2.

$$f_i^W = x_i^W f_i^{oW} \quad (3.17)$$

Where

$$f_i^{oW}(P) = f_i^{oL}(P) \exp \left(-\frac{\Delta H_i^f}{RT} \left[1 - \frac{T}{T_i^f} \right] - \frac{1}{RT} \int_T^{T_i^f} \Delta C_{p_i} dT + \frac{1}{RT} \int_T^{T_i^f} \frac{\Delta C_{p_i}}{T} dT + \frac{\Delta V_i(P - P_{ref})}{RT} \right) \quad (3.18)$$

Pedersen simplified this pure component fugacity equation by neglecting the heat capacity difference ΔC_{p_i} between the solid-wax and the liquid phase of equation (3.18) while the enthalpy of fusion and the temperature of fusion is calculated by the Won's description of fusion enthalpy and the fusion temperature in equation (3.6) respectively[10].

Further hypothesis for handling the liquid-vapour phase in equilibrium with the wax phase was accounted in the work of Pedersen (1995). He put forward the Soave-Redlich-Kwong cubic equation of state to calculate the liquid and vapour state fugacity coefficient respectively.

The liquid fugacity and gas fugacity is thereby expressed by the fugacity coefficient ϕ_i , pressure P and the mole fraction x_i of component i in the liquid and the vapour phase respectively as defined by equation (3.19) and (3.20)[10].

$$f_i^L = x_i^L \phi_i^L P \quad (3.19)$$

$$f_i^V = x_i^V \phi_i^V P \quad (3.20)$$

The fugacity of pure component i f_i^{oL} in the liquid phase is specified by equation (3.21) where $\phi_i^{oL}(P)$ is the fugacity coefficient of pure liquid component at pressure P . The fugacity coefficient ϕ_i of the liquid and vapour phases is calculated by the SRK fugacity coefficient equation recorded in Appendix 10.3.

$$f_i^{oL} = \phi_i^{oL}(P)P \quad (3.21)$$

Combining equation (3.17) of the wax fugacity, the equation (3.21) of the pure component fugacity of component i in the liquid phase with the wax fugacity equation in (10.25) of Appendix 10.2, the wax fugacity can be expressed by equation (3.22) using the pure liquid fugacity coefficient at pressure P .

$$f_i^W = x_i^W \phi_i^{oL}(P)P \exp\left(-\frac{\Delta H_i^f}{RT}\left(1-\frac{T}{T_i^f}\right) + \frac{\Delta V_i(P-P_{ref})}{RT}\right) \quad (3.22)$$

The change in molar volume parameter associated with the Pedersen fugacity equation represents a volume decrease in the phase change solidification process as supported by experimental observation of Templin (1956)[10].

C₇₊ Characterisation procedure of Pedersen et al is used to determine associated cubic equation of state parameters (T_c, P_c , and ω) such that wax forming part and non-wax forming parts are assigned different critical pressures using the equation (3.23) to calculate for each *pseudo* component i in the mixture[10].

$$P_{ci}^W = P_{ci} \left(\frac{\rho_i^P}{\rho_i}\right)^{3.46} \quad (3.23)$$

Where P_{ci} is the critical pressure of pseudo component i obtained from the Pedersen et al characterisation consisting of the wax forming and the non-wax forming components, ρ_i the average density of component i consisting of the wax forming and the non-wax forming part, and ρ_i^P is the density of the wax forming paraffin as defined in equation (3.15).

The critical pressure of the non-wax forming part P_{ci}^{nonW} of component i obtained from characterisation is obtained by fixing in the critical pressure of the wax-forming component in equation (3.24).

$$\frac{1}{P_{ci}} = \frac{\left(\frac{z_i^{tot} - z_i^W}{z_i^{tot}} \right)}{P_{ci}^{nonW}} + \frac{\left(\frac{z_i^W}{z_i^{tot}} \right)^2}{P_{ci}^W} + \frac{2 \frac{z_i^{tot} - z_i^W}{z_i^{tot}} \times \frac{z_i^W}{z_i^{tot}}}{\sqrt{P_{ci}^{nonW}} \sqrt{P_{ci}^W}} \quad (3.24)$$

Critical pressure compared for the wax and the non-wax forming parts derived from equation (3.23) and (3.24) respectively indicate a lower critical pressure for the wax forming part. This agrees with a low critical pressure of n -paraffin when compared to the critical pressure of aromatic and naphthenic of same molecular weight[10].

The reliability of this model steers from its ability to differentiate wax forming components and the non-wax forming components while using an equation of state model to determine the critical properties obtained from the equation of state characterisation. It's simplification of wax oil mixtures as ideal is questioned as is understood that in real hydrocarbon mixtures, solid-wax interactions and oil-wax non-ideality interactions exist between molecules in phase transitions.

3.5. Lira-Galeana et al Multi-Solid Model

This multi solid wax model hypothesis is based on the grouping of hydrocarbon components using average properties assigned to components or pseudo components fractions in oil mixtures[37]. Lira-Galeana et al (1996) based his theory on explanations that n -paraffin, iso -paraffin and naphthalene are the primary wax formers and that aromatics do not participate as precipitating solid in the wax phase therefore average distinguishing properties should be assigned to respective group species[8].

Phase equilibrium descriptions of the multi-solid model employ the Won's model description of the wax fugacity obtained by equation (3.12) as described in Section 3.1 and the Pedersen equation of state model for the liquid fugacity – equation (3.19) and (3.20) but he used different correlations to calculate the melting temperature, the enthalpy of fusion and the heat capacity differences for the naphthalene and the aromatic components as against average properties used by Won and Pedersen models.

The melting enthalpy and the melting temperature of the n -paraffin part is calculated by equation (3.25).

$$\Delta H_i^f = 0.142M_iT_i^f; \quad T_i^f = 374.5 + 0.0261M_i - \frac{20172}{M_i} \quad (3.25)$$

Similarly, the naphthalene and the aromatic component is calculated by equation (3.26)[37].

$$\Delta H_i^f = 0.05276M_iT_i^f; \quad T_i^f = 333.5 - 419 \exp(-0.00855M_i) \quad (3.26)$$

The heat capacity of fusion for all components i is calculated by equation (3.27)[37].

$$\Delta C_{pi} = 0.3033M_i - 4.635 \times 10^{-4} M_iT_i^f \quad (3.27)$$

Critical properties for the light hydrocarbon parts are obtained using the Two (1984) correlations and from the more recent work of Riazi and Al-Sahhaf (2008) while equation (3.28) calculates the critical pressure of components with higher than 300g/mol molecular weight[37, 38]. The critical property of heavy components is calculated by the correlations of Riazi and Al-Sahhaf (2008)[37].

The acentric factor for aromatic component i is obtained by equation (3.29). For components with molecular weight $M_i > 800$, the acentric factor is assumed equal to 2 while the acentric factor for paraffin and naphthalene correlations is obtained from the Riazi and Al-Sahhaf (2008)[37].

$$P_{c,i} = A - B \exp(-CM_i) \quad (3.28)$$

Where A, B and C are constants given in Table 3-2.

$$\ln \omega_i = -36.1544 + 30.94M_i^{0.026261}; \quad M_i \leq 800 \quad (3.29)$$

Table 3-2 Constant for Parameters A, B and C in equation (3.28).

Parameter	Paraffins	Naphthens	Aromatics
A	0.06799	2.588	4.85
B	- 22.18	-27/629	- 42.93
C	0.00284	0.0045	0.00561

The multi-solid model prediction agrees with the increasing effect of pressure on WAT as with the Pedersen model as well as the decreasing effect of light component on WAT. However, there are curiosities about its not distinguishing non-wax and wax forming parts in the PNA model. Question also remains about the effect of further subgrouping of pseudo-components in the multi solid model.

3.6. Predictive Uniquac thermodynamic model

The Coutinho et al (2006) thermodynamic model utilizes the solution behaviour of *n*-paraffin molecules in the oil phase. It describes a local predictive compositional properties for the thermodynamic of wax-oil system using cubic equation of state for wax-oil equilibrium calculations[9].

The predictive thermodynamic work of Coutinho has been based on prior-work of Wilson and a more developed predictive version of the Uniquac model called the Predictive Uniquac model that accounts for solid-solid thermodynamic interactions and solid-solid phase transition in wax-oil solutions.

Assumptions of the Coutinho model are based on the premise that ideal solutions with activity coefficient of 1 are under simplification of equilibrium systems for hydrocarbon mixtures. It argues the non-ideal behaviour of hydrocarbon mixtures due to entropic differences, size differences, free volume effect and energetic interactions between unlike molecules such as the aromatics and the aliphatic. It further presents a non-ideality formulation – a modification for the activity coefficients as characteristic of the liquid non-ideality and the solid (wax) non-ideality for components present in hydrocarbon mixture[33, 39].

The liquid phase non-ideality $\ln \gamma_i^L$ is expressed by a free volume effect to account for size differences defined in the Flory-free volume equation of (3.31) and a residual characteristic defined by a modified Uniquac model which describes energetic interaction effects between unlike molecules[9].

$$\ln \gamma_i^L = \ln \gamma_i^{res} + \ln \gamma_i^{comb-fv} \quad (3.30)$$

$$\ln \gamma_i^{comb-fv} = \ln \frac{\phi_i}{x_i} + 1 - \frac{\phi_i}{x_i}; \quad \phi_i = \frac{x_i \left(V_i^{\frac{1}{3}} - V_{wi}^{\frac{1}{3}} \right)^{3.3}}{\sum_j x_j \left(V_j^{\frac{1}{3}} - V_{wj}^{\frac{1}{3}} \right)^{3.3}} \quad (3.31)$$

Where V_i is the molar volume and V_{wi} is the Van der Waals volume of component i .

The wax phase non-ideality defined by Wilson equation of the excess Gibbs free energy G^E for solid solution of n -paraffin is obtained in equation (3.32) where n_i^W and x_i^W is the mole number and mole fraction of component i in the wax phase respectively.

$$\frac{G^E}{RT} = - \sum_i n_i^W \ln \left(\sum_j x_j^W \exp(\lambda_{ji} - \lambda_{ii}) \right) \quad (3.32)$$

The Wilson parameters λ_{ji} and λ_{ii} are calculated by equation (3.33) such that $\Delta H_{sub,i}$ is the sublimation enthalpy of component i which is the sum of the enthalpy of fusion and the enthalpy of vaporisation at the melting point. $\Delta H_{sub,i} = \left| \Delta H_i^f + \Delta H_i^v \right|_{meltingpoint}$ and α_{ij} is the Wilson correction factor taking into account end effects in wax crystal[9].

$$\lambda_{ji} = \alpha_{ij} \min(\lambda_{ii}, \lambda_{jj}); \quad \lambda_{ii} = -\frac{1}{3}(\Delta H_{sub,i} - RT) \quad (3.33)$$

$$\alpha_{ij} = 1 - 8 \times 10^{-7} \left| \Delta H_{sub,i} - \Delta H_{sub,j} \right| \quad (3.34)$$

The Wilson model is recorded to have produced good prediction of the amount of wax and the WAT but it is limited by making wax a single solid solution as opposed to theory that accounts that wax crystals is a combination of multiple solid wax phases.

To overcome the single solution of the solid phase in the Wilson's model, Coutinho developed a multi-solid solution model using the predictive Uniquac analysis obtained from the calculation of thermo physical properties for the excess Gibbs free energy G^E [9]. He proposed associated transition correlations in thermo physical definitions of melting properties of the wax phase to account for

rotator to orthorhombic phase transitions of precipitated n -paraffin from their concentrated solution[33, 39].

The predictive Uniquac excess Gibbs free energy is obtained by equation (3.35) correlations and the Uniquac parameters for components i are obtained from equation (3.36)[9].

$$\frac{G^E}{RT} = \sum_i n_i^W \left[\ln \left(\frac{r_i}{\sum_j x_j^W r_j} \right) + 3q_i \ln \left(\frac{q_i \sum_j x_j^W r_j}{r_i \sum_j x_j^W q_j} \right) - q_i \ln \left(\frac{\sum_j x_j^W q_j \exp(\lambda_{ji} - \lambda_{ii})}{\sum_j x_j^W q_j} \right) \right] \quad (3.35)$$

$$q_i = 0.1N_i + 0.1141; \quad r_i = 0.1N_i + 0.0672 \quad (3.36)$$

Where N_i is the carbon number of component i . The cross term λ_{ji} between component i and j represents the interaction energies between two non-identical molecules such that $\lambda_{ji} = \min(\lambda_{ii}, \lambda_{jj})$ [9, 33]. The interaction energy λ_{ii} between two identical molecules calculated by equation (3.37) is estimated from the heat of sublimation $\Delta H_{sub,i}$ of pure wax in the orthorhombic phase[33].

$$\lambda_{ii} = -\frac{2}{Z}(\Delta H_{sub,i} - RT) \quad (3.37)$$

Where Z is the coordination number equivalent to the value 6 for orthorhombic crystals[33]. The enthalpy of sublimation is obtained as the sum of the enthalpy of fusion, the enthalpy of vaporisation and the transition enthalpy of component i at the melting point[33].

$$\Delta H_{sub,i} = \left| \Delta H_i^f + \Delta H_i^v + \Delta H_i^{tr} \right|_{meltingpoint} \quad (3.38)$$

The enthalpy of fusion and melting temperature in Kelvin for n -paraffin greater than tetraoctane n -C₄₀ is obtained by equation (3.39) and (3.40) giving the change in Gibbs energy equation of (3.41) where T is the absolute temperature[9].

$$\Delta H_i^f = 3779.1N - 12654 \text{ J/mol} \quad (3.39)$$

$$T_i^f = 421.3 - 1936412 \exp\left(-7.8945(N-1)^{0.07194}\right) \quad (3.40)$$

$$\Delta G = \Delta H_i^f \left(\frac{T}{T_m} - 1 \right) \quad (3.41)$$

n-paraffin between octane *n*-C₈ and tetraoctane *n*-C₄₀ is observed to exist as a rotator phase at the melting point and consist of more complicated phase transitions[9]. The melting temperature and the enthalpy of fusion for this rotator phase is giving by equation (3.40) and equation (3.42) respectively.

$$\Delta H_i^f = 3.55N^3 - 237.6N^2 + 7400N - 34814 \text{ J/mol} \quad (3.42)$$

Associated transition Enthalpy of component *i* from the rotator phase to the orthorhombic is obtained as the difference between the Enthalpy of fusion in the rotator phase and Enthalpy of fusion in the orthorhombic phase. The transition temperature of solid waxes can likewise be derived with equation (3.43)[9].

$$T_i^{rr} = 420.42 - 134784 \exp\left(-4.344(N + 6.592)^{0.14627}\right) K \quad (3.43)$$

The change in Gibbs free energy is calculated hence

$$\Delta G = \Delta H_i^f \left(\frac{T}{T_i^f} - 1 \right) + \Delta H_i^{rr} \left(\frac{T}{T_i^{rr}} - 1 \right) \quad (3.44)$$

Phase equilibrium relation between the wax phase and the oil phase is coupled using cubic equation of state equations for *n*-paraffin in the respective phases. The Gibbs free energy of the solid wax phase is obtained as the sum of the Gibbs energy in the liquid phase obtained from the equation of state correlations, the Gibbs energy of fusion and the excess Gibbs energy of wax phase[9].

$$G_i^W = G_i^L + G_i^f + G^E \quad (3.45)$$

The fugacity of component *i* $f_i = x_i \phi_i P$ defined by the fugacity coefficient ϕ_i at pressure *P* is obtained from equation (3.46) where *n_i* is the mole number of component *i*, *G* is the Gibbs free energy for the

phase and G^{id} is the Gibbs free energy of the ideal gas phase of same composition same temperature and pressure[9].

$$\ln \phi_i = \frac{\partial}{\partial n_i} \left(\frac{G - G^{id}}{RT} \right) \quad (3.46)$$

The predictive Uniquac model gives reliable predictions for live oil over wide range of temperatures with its major benefit is its use of an equation of state to describe the fluid phases and its wax-equilibrium calculation at high pressure over ranges of temperatures[9]. Although, the results from the model shows excellent agreement with Rønningsen oil collection of dead oils and its agreement with observed report of live oil, curiosity arises on how the model justifies the contributions of n -paraffin below octane n -C₈ that are not accounted for in the thermo physical correlations. Since there are no differentiation of wax forming part and non-wax forming part, it is also thought that the non-wax forming part will induce a depressing effect of the WAT and as well on the equilibrium prediction by the equation of state.

4. Problem Description and the OLGA model

Considerable effort has been carried out over the last decade to provide process solution for reservoir fluids with high wax content. A great deal of this effort has been directed to developing models in process simulators that predicts wax deposition in the pipelines. Such is intended to provide information needful to plan wax management or wax remediation strategies. As rightly discussed in Section 1.2, these present wax management strategies is largely inapplicable to long, deep and harsh environment's production developments as they are expensive at present economic realities.

Experimental results from the Porsgrunn flow loop of Statoil AS reveals that stable wax solid is released from wax deposits on pipeline walls when the inner wall is heated for a short period of time such that released stable wax is transported in the cool stream without re-deposition downstream the flowline[19]. Heating of the pipeline is suggested to be either by electric heating, inductive heating or by flowing a warm fluid exchanging heat with the deposited wax through a heat exchanger or an annulus[19].

Presently there are no records of process modelling work that have performed this cold flow wax control in process simulators. This work attempts to bridge this gap by presenting tested case of wax deposition simulation as well as wax loosening simulation performed in the OLGA simulator. This chapter also describes the underlining wax models implemented in OLGA, the case inputs into OLGA simulation obtained from PVTsim – a tab generating PVT package and outlines the basis for the wax deposition and wax control simulation performed in OLGA in this thesis.

4.1. The OLGA wax module

OLGA is a dynamic multiphase simulator employed for transient and steady state simulations in wells and flowlines. OLGA is owned by the SPT Group but continuously verified for improved accuracy by the SPT Group and its sister joints project initiatives. The OLGA is structured into modules and includes a wax deposition module that is commercially used for wax precipitation prediction and wax deposition calculations in the oil and gas industry.

The OLGA wax deposition module is a steady state simulator module because of the slow wax deposition process time relative to other active process time within the pipeline. The wax module consists of three-implemented models for wax prediction and deposition calculation. They are the RRR model, the Matzain model and a Heat Analogy model. The RRR and the Matzain deposition model have been discussed in Section 2.2.1 and 2.2.2 respectively. Thermodynamic and precipitation

descriptions of the Heat Analogy model have not being discussed in this thesis because of the unavailability of documentation describing it but it is assumed that the Heat Analogy model will in principle be similar to the Singh et al wax deposition principles employing heat and mass balances coupled with energy balances for its wax precipitation and deposition predictions. Wax deposition simulations performed in this work are done using the OLGA 7.1.4 version of the OLGA simulator.

OLGA receives its propriety input values from tab files generated from tab generating PVT package such as the PVTsim. Tab files supplied to OLGA contain tabulated values of fluid properties (density, compressibility, viscosities, surface tension, enthalpies, heat capacities, and thermal conductivity) in pressure and temperature values[40]. All tab files generated for this thesis simulation has been produced using the SRK Peneloux cubic equation of state from the PVTsim simulator package. Similar results could as well be obtained from the PR cubic equation of state in the PVTsim package.

The wax deposition module in OLGA further requires a wax file in a tab format generated from the PVTsim wax interface. The wax file provides information on the wax fraction as function of the wax forming components, temperature, pressure and other thermo physical properties of the oil and wax mixture.

Possible tuning of WAT and the wax in STO to experimental values can potentially be carried out in PVTsim but this thesis did not focus on the effect of such tuning on wax prediction of the simulator. Wax phase envelope and a no-wax phase envelope could as well be obtained to give a better understanding of the pressure temperature equilibrium relationship of the oil fluid. Results and prediction of the OLGA simulator is largely influenced by the accuracy of tables' values generated from PVTsim hence the need for appropriate tuning and characterisation of the oil in the PVTsim package. A description of the simulation procedure in the PVTsim and the OLGA simulator is further presented in the sections below.

4.2. Definition of terms in PVTsim

A hypothetical fluid from a typical production oil field with subsea production flowline for subsea transport of oil is created for wax simulation. The oil is imputed into PVTsim for characterization; where molar concentration of characterized fluid is obtained. Composition of the characterized oil from the PVTsim package is shown in the composition analysis of Table 4-1. The characterization of C₇₊ fraction using the SRK Peneloux cubic equation of state is required to obtained the critical

properties of component i in the oil-wax mixture as well as it is required for the lumping of the heavy compounds into pseudo components.

Table 4-1 Fluid Composition of oil used for PVTsim and OLGA simulation

Component	Mol %	Mol wt	Liquid Density (g/cm ³)
C ₁	0.418	16.043	
C ₂	0.059	30.07	
C ₃	0.367	44.097	
<i>i</i> C ₄	0.206	58.124	
<i>n</i> C ₄	0.849	58.124	
<i>i</i> C ₅	0.69	72.151	
<i>n</i> C ₅	1.184	72.151	
C ₆	3.794	86.178	0.664
C ₇	8.42	97.32	0.738
C ₈	9.096	114.232	0.765
C ₉	11.636	128.258	0.781
C ₁₀ -C ₁₂	20.378	146.475	0.7834
C ₁₃ -C ₁₅	10.715	189.347	0.7863
C ₁₆ -C ₁₇	5.614	229.142	0.7883
C ₁₈ -C ₂₀	6.643	262.236	0.79
C ₂₁ -C ₂₄	6.355	309.664	0.7921
C ₂₅ -C ₂₈	4.335	364.784	0.7941
C ₂₉ -C ₃₃	3.537	427.333	0.796
C ₄₃ -C ₈₀	3.329	519.186	0.7983

Pseudo components between C₁₀ to C₈₀ are present as mixture components as revealed by composition analysis of Table 4-1. The moderate density values of the oil composition suggest its

paraffinic nature and therefore suggest a seemingly tendency for wax deposition when cooled below the WAT. The subsea flowline is further considered for potential wax challenges as properties of the oil and analysis from the PVTsim package predict a WAT of 32.8°C having 17.253 weight percent of wax in stock tank oil.

The phase envelope for oil is shown in Figure 4-1. It reveals a critical point of 446.21°C at 35.17bar. Liquid fractions are present in the hydrocarbon mixture at all temperature conditions below this critical temperature. This suggests the presence of heavy fractions and the stable properties of the liquid phase at high temperatures.

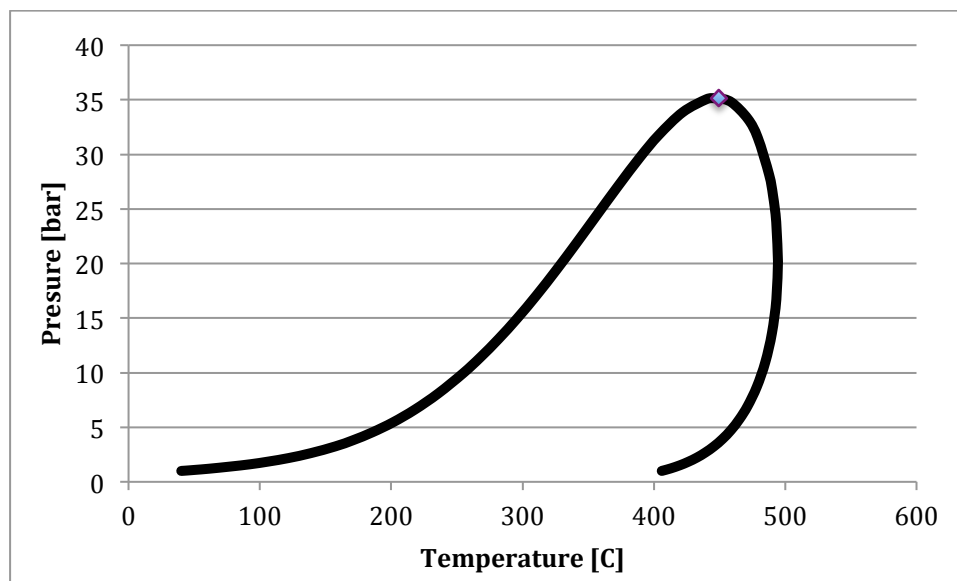


Figure 4-1 Phase envelope of the oil used for wax simulations

A PT flash calculation to determine the various phases present in the mixture is simulated at standard condition as recorded in Table 4-2. Similarly an extended phase split of the PT flash calculation is obtained as shown in result from Table 4-3. Table 4-2 and Table 4-3 reveals that C_{10} , C_{25} - C_{28} and the C_{29} - C_{33} plus fractions as the dominating heavy fraction in the mixture. C_{43} - C_{80} fractions obtained with low molar percent indicates its minimum contribution in the wax phase. It rightly confirms the experimental work of Pedersen et al (2007) that C_{50+} compounds have no considerable effect on wax formation in oil and gas productions. The properties of the PT flash calculation of the oil and wax phase is recorded in Table 4-4.

Table 4-2 PT Flash Composition of oil in mole% at 1.013bar, 15°C

	Total	Liquid	Wax
C ₁	0.418	0.428	0.000
C ₂	0.059	0.061	0.000
C ₃	0.367	0.376	0.000
<i>i</i> C ₄	0.206	0.211	0.000
<i>n</i> C ₄	0.849	0.870	0.000
<i>i</i> C ₅	0.690	0.707	0.000
<i>n</i> C ₅	1.184	1.214	0.000
C ₆	3.794	3.889	0.000
C ₇	8.420	8.621	0.339
C ₈	9.096	9.312	0.416
C ₉	11.636	11.910	0.624
C ₁₀	63.282	62.400	98.621
C ₁₀₊ Molwt	261.5	256.9	378.2

Table 4-3 Extended PT Flash Composition in mole% at 1.013bar, 15°C

	Total	Liquid	Wax
C ₁	0.418	0.428	0.000
C ₂	0.059	0.061	0.000
C ₃	0.367	0.376	0.000
<i>i</i> C ₄	0.206	0.211	0.000
<i>n</i> C ₄	0.849	0.870	0.000
<i>i</i> C ₅	0.690	0.707	0.000
<i>n</i> C ₅	1.184	1.214	0.000
C ₆	3.794	3.889	0.000
C ₇	8.420	8.621	0.339
C ₈	9.096	9.312	0.416
C ₉	11.636	11.910	0.624
C ₁₀	63.282	62.400	98.621
C ₁₀ -C ₁₂	20.378	20.848	1.528
C ₁₃ -C ₁₅	10.715	10.932	1.99
C ₁₆ -C ₁₇	5.614	5.692	2.47
C ₁₈ -C ₂₀	6.643	6.661	5.925
C ₂₁ -C ₂₄	6.355	6.124	15.605
C ₂₅ -C ₂₈	4.335	3.842	24.087
C ₂₉ -C ₃₃	3.537	2.687	37.572
C ₃₄ -C ₄₂	3.329	3.177	9.435
C ₄₃ -C ₈₀	2.376	2.435	0.006

Table 4-4 PT Flash Properties of Oil at 1.013bar, 15°C

	Total	Liquid	Wax	Units
Mole%	100	97.56	2.44	
Weight%	100	95.54	4.46	
Volume	261.09	257	424.96	cm ³ /mol
Volume%	100	96.04	3.96	
Density	0.7832	0.7791	0.8815	g/cm ³
Z Factor	0.011	0.0109	0.018	
Molecular Weight	204.48	200.24	374.59	
Enthalpy	-69592	-66668.1	-186742.4	J/mol
Entropy	-116.47	-109.41	-399.46	J/mol C
Heat Capacity (C _p)	443.51	434.26	814.02	J/mol C
Heat Capacity (C _v)		408.33		J/mol C
Kappa (C _p /C _v)		1.064		
JT Coefficient		-0.0501		°C/bara
Velocity of Sound		1159.3		m/s
Viscosity		8.386		cP
Thermal Conductivity		121.862	200	mW/m C
WAT			32.8	°C
Wax in STO	17.253			Weight %
Volume, Enthalpy, C _p and C _v are per mole phase				

Wax in STO is the weight% of wax precipitated from the stock tank oil cooled down to 223.15K/-50.15°C[28]; The Stock Tank Oil is the oil obtained from a flash composition at 15 °C and 1.013 bara[28].

Wax formation curve is further obtained from PVTsim as shown in Figure 4-2. The wax formation curve shows the simulation results of the weight percent of wax with temperature at 1bar, 15bar and 100bar respectively. The PVTsim result is shown in Table 4-5.

The wax formation curve shows approximate increase of the WAT with pressure, although this increase is fairly insignificant over operating pressure range between 1 and 100bar considered. A WAT-pressure calculation at higher pressures is shown in Figure 4-3. This confirms the increases in WAT with pressure, the stable properties of the oil and the absence of dissolved gasses or other wax depressing composition in the fluid mixture.

Table 4-5 Wax formation data from PVTsim simulation

Wax Formation at 1bar		Wax Formation at 15bar		Wax Formation at 100bar	
Temperature	Weight% wax	Temperature	Weight% wax	Temperature	Weight% wax
°C		°C		°C	
33.06	0	33.31	0	33.95	0
18.28	3.605	18.5	3.616	19.07	3.645
3.49	7.206	3.69	7.223	4.18	7.264
-11.29	10.322	-11.12	10.342	-10.7	10.392

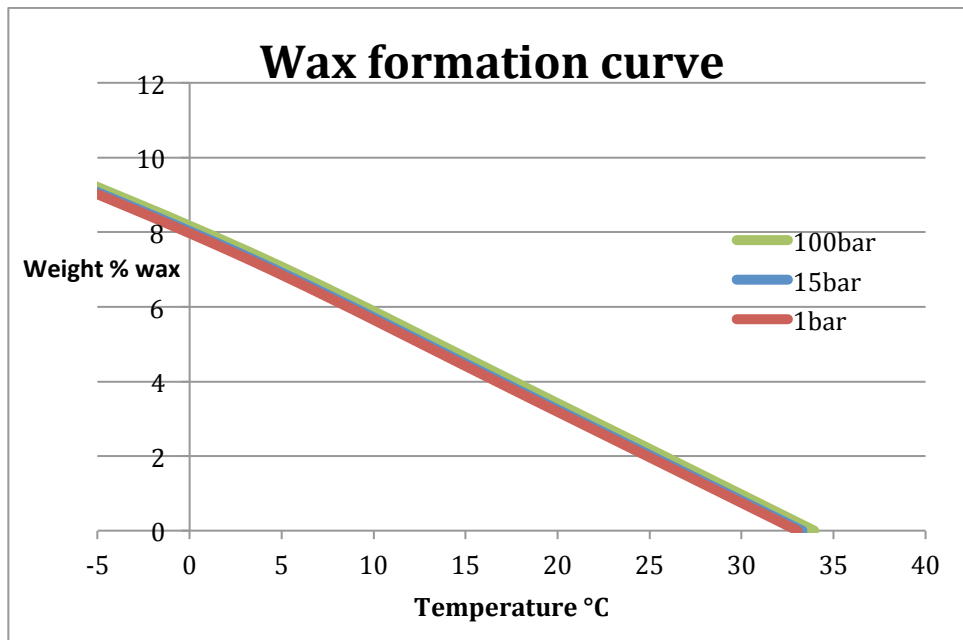


Figure 4-2 Oil wax formation curve obtained from PVTsim simulation

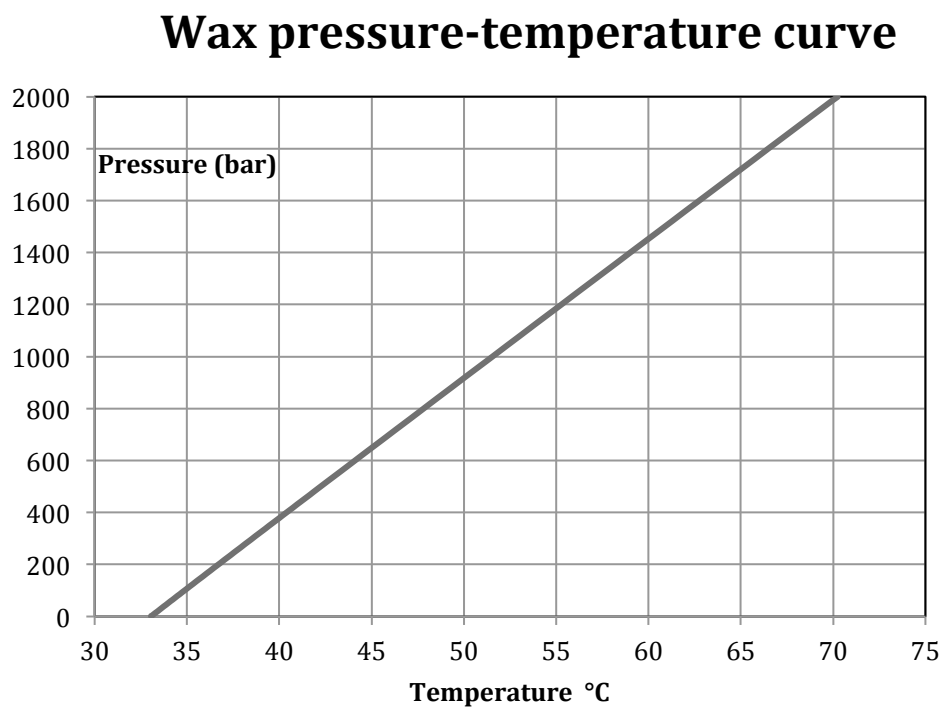


Figure 4-3 Wax pressure-temperature curve

As indicated in the description of the OLGA wax module in Section 4.1 above, tuning of this wax formation curve to the observable wax in stock tank oil is not considered. This simulation model rather focuses on process solution for depositing wax in oil and gas process streams and as such

emphasis here is not on wax precipitation concentration in the bulk fluid. A more adequate analysis on the effect of the tuning of the wax formation curve on wax precipitation concentration is considered in the work of Labes-Carrier, C., et al. (2002)[15].

4.3. Definition of terms in OLGA

To start with, the first fundamental step of process simulation rest on the selection of appropriate thermodynamic model that accurately predicts thermodynamic properties of both the oil and the solid wax in the simulation. The Pedersen (1995) wax model is selected for thermodynamic prediction of wax precipitation. The Pedersen model is selected because it is based on the thermodynamic properties of wax-oil mixtures consisting of wax forming parts and non-wax forming parts. The model is implemented in the PVTsim simulator. The wax model is used with the SRK Peneloux cubic equation of state for the characterisation of the oil. It is also used to obtain the associated equation of state parameters in the gas phase. The SRK Peneloux cubic equation is selected for the characterisation to account for volume correction of liquid densities using a volume shift parameter associated with the equation of state. The gas fugacity coefficient is obtained from the SRK Peneloux cubic equation prediction to determine the equilibrium concentration of predicted wax in Table 4-2.

Careful importance is given to determine the phase behaviour of the wax in the oil and the non-wax forming parts in the wax-oil solution. The PT flash performed at 1.013bar and 15°C reveals the absence of volatile fractions and the high C₁₀ fractions. Wax solubility curves obtained from PVTsim provide analysis of wax concentration expected in the OLGA model at different pressure.

For the flowline wax deposition modelling in OLGA, the RRR wax model is preferred to the Matzain and the Heat Analogy model because it produces a consistent increase of the continuous estimate of the wax build-up over integration of time for multicomponent mixtures. This is rightly observed from the work of Ajayi E. O (2013) shown in Figure 10-1 of appendix 10.4[7]. The trend prediction from the Matzain model gave a much higher prediction of wax thickness than that predicted by the RRR and Heat Analogy model. A simulation verification to confirm the over prediction of the Matzain model is carried out on the oil with verification result shown by the profile plots of Figure 4-4.

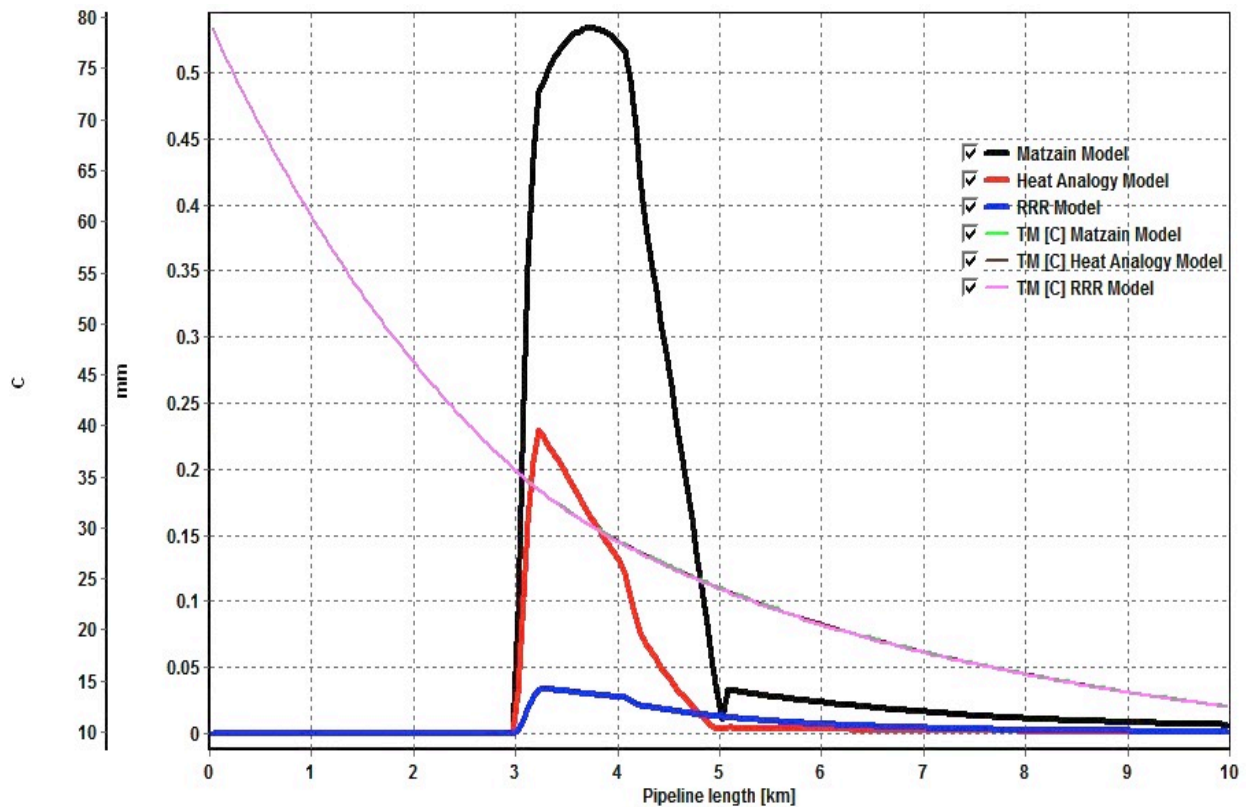


Figure 4-4 Profile plot of wax thickness for RRR, Matzain and Heat Analogy model after 2 days

The over prediction of the wax thickness of the Matzain model is attributed to incorporated deposition enhancing coefficients introduced into the Matzain correlations. This enhancement coefficient is believed to account for other wax deposition enhancing mechanism, which the diffusion coefficient and the shear dispersion coefficient could not validate.

Although the RRR model predicts a conservative result when compared with the Matzain and the Heat Analogy model, the ability to initiate a dissolution possibility in RRR model coupled with the consistency of its prediction influenced the selection of the model. At present, there exist no dissolution possibility in the Matzain and the Heat Analogy model in the wax module of OLGA.

5. Results and Discussion of Controlled Wax Simulations

Wax deposition models predict deposition thickness of the wax at the wall as a measuring parameter of the severity of wax deposited in the oil and gas flow systems. This thesis relies on this premise as it present wax thickness results to justify wax performance on simulations implemented. Thermo hydraulic representation of the flowline is first presented followed by wax deposition modeling and wax control models simulated. Cases simulated are listed in Table 5-1.

Table 5-1 Simulation cases in OLGA

Simulation case	Oil flow rate		Water flow rate
Thermohydraulic verification case	500Sm ³ /day		-
Base case	500Sm ³ /day		-
Co-current cooling case	Case A	Case B	5000Sm ³ /day
	500Sm ³ /day	5000Sm ³ /day	
Counter current cooling case	Case A	Case B	5000Sm ³ /day
	500Sm ³ /day	5000Sm ³ /day	
Wax liberation case	5000Sm ³ /day		5000Sm ³ /day of hot water

5.1. Thermohydraulic simulation

A steady state simulation is performed to validate the thermohydraulic properties of the flowline prior to wax deposition simulation. The tab file generated from PVTsim with tabulated properties of the oil given in Table 4-1 is imputed to OLGA as a PVTFIL. A 6inch subsea flowline is modeled to transport this oil from a typical production well represented as a mass source called Oil Source in the first node of PIPE-1 into the flowline as shown in Figure 5-1. The oil flows out of the flowline at 50bars and 10°C through a pressure node called the Oil Outlet in Figure 5-1 where mass and energy interaction are represented by pressure condition of the node. The flowline also consists of a closed node with no mass and energy transfer on PIPE-1 of the flowline.

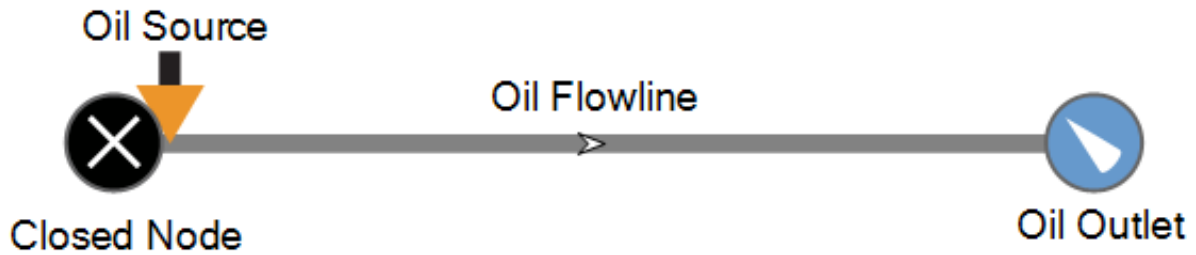


Figure 5-1 Schematic flowline diagram

The geometry of the flowline is a combination of ten equal pipelines, each pipeline discretised into grids of 20 sections as detailed in Table 5-2. An assumption of near horizontal level is made for this geometry; height-induced effect and flow regime changes are therefore not considered.

Table 5-2 Oil flowline geometry

Pipe	x	Y	Length	Elevation	Section	Diameter
	[m]	[m]	[m]	[m]		[m]
Start Point	0	-100				
PIPE-1	1000	-100	1000	0	20	0.1503
PIPE-2	1000	-100	1000	0	20	0.1503
PIPE-3	1000	-100	1000	0	20	0.1503
PIPE-4	1000	-100	1000	0	20	0.1503
PIPE-5	1000	-100	1000	0	20	0.1503
PIPE-6	1000	-100	1000	0	20	0.1503
PIPE-7	1000	-100	1000	0	20	0.1503
PIPE-8	1000	-100	1000	0	20	0.1503
PIPE-9	1000	-100	1000	0	20	0.1503
PIPE-10	1000	-100	1000	0	20	0.1503

A solid type pipeline material made of carbon steel with a heat transfer coefficient of about a $6.8\text{W/m}^2\text{-C}$ is selected as the flowline material. Other heat transfer property of the flow line is given in Table 5-3.

Table 5-3 Pipe material for oil flowline

	Thickness	Conductivity	Density	Heat Capacity
	[m]	[W/m-k]	[Kg/m3]	[J/Kg-k]
Carbon Steel	0.2362	45	7850	470

The simulation case time is set at 70 days. The time setup also requires setting maximum and minimum integration time step to control simulation time step based on the Courant-Friedrich-L Levy criterion[40]. The maximum and minimum integration time steps are set to 0.5 and 0.001 seconds respectively. Other simulation definition and input values are detailed in Table 5-4.

Table 5-4 Input data into thermo hydraulic verification simulation

Parameter	Value
Flowline length	10km
Fluid	Oil
Oil Inlet temperature	80°C
Standard flow rate	500Sm ³ /day of Oil
Mass flow rate of oil	4.49kg/s
Oil velocity	0.34m/s
Seabed temperature	6°C
Fluid Density	0.7829g/cm3

Representation of the pressure, temperature and geometry of the flowline is shown in Figure 5-2. Inlet temperature of the oil in PIPE-1 is specified to be 80°C while temperatures and pressure of the oil outlet source is fixed to 10°C and 50bar respectively.

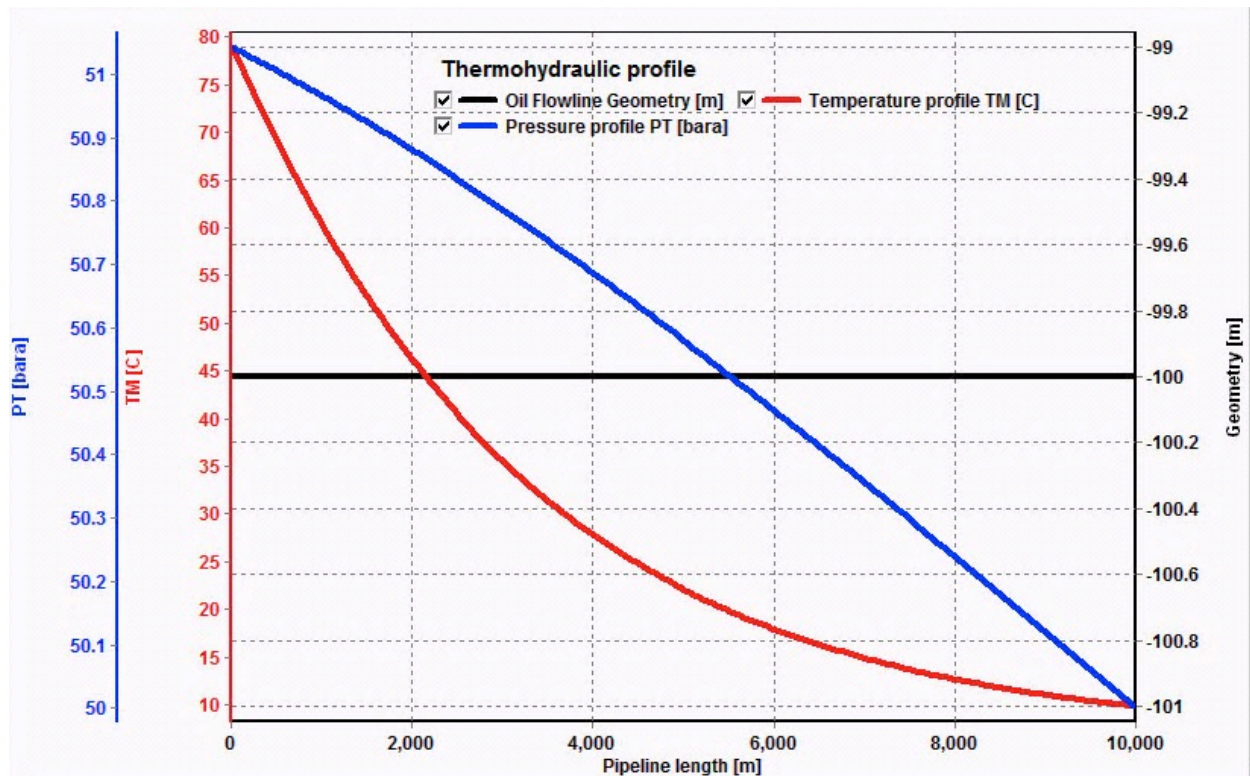


Figure 5-2 Pressure, temperature and geometry representation of the flowline

Results obtained for this thermohydraulic simulation of the flowline shown in Figure 5-2 indicate a 1bar pressure drop and a 70°C temperature drop in the flowline. It as well provides a reasonable guess of anticipated pressure and temperature drop performance of the flowline during wax deposition. The large temperature drop in this thermohydraulic suggests expected temperature drop as well as an anticipated higher pressure drop in the wax deposition simulation.

5.2. Base case for wax deposition simulation

The OLGA wax deposition option is turned ON and the verified thermohydraulic model described in Section 5.1 is updated for wax deposition simulation. Input parameter for this wax deposition case is recorded in Table 5-5.

Table 5-5 Input data into base case wax deposition simulation

Parameter	Value
Wax deposition model	RRR
Wax diffusion coeff. multiplier	1
Wax roughness:	0
Wax porosity	0.6
Viscosity (wax/oil dispersion)	CALSEP
WAT	32.8°C
Seabed temperature	6°C
Simulation end time	70days

Figure 5-3 shows the base case wax deposition profile along the 10km flowline. Profiles in the figure include the wax appearance temperature, the specific wax mass at the wall, the oil temperature, the oil pressure and the wax thickness after 70 days simulation. Wax does not precipitate out of the oil, upstream the pipeline when the oil temperature is above the WAT. As the oil temperature cools below the WAT, a sharp growth in the amount of wax precipitated is observed resulting in the high value of the specific mass of wax at the wall. The specific wax mass on the wall is seen to exhibit a comparable relationship with the wax thickness and could potentially be used to describe wax performance in the flowline.

Bulk of the wax deposited is observed in PIPE-4 – Section-1 where the oil temperature crosses below the WAT. Further downstream the flowline, the wax thickness and the specific mass at the wall gradually reduces, with decreasing oil temperature to 10°C. This is due to the low thermal gradient existing between the flowing oil and the ambient temperature. This principle of wax deposition as a consequence of a necessary temperature gradient between the bulk fluid and a surrounding ambient fluid is simulated in the sections below as an important flow assurance concept for handling wax deposition in subsea flowlines.

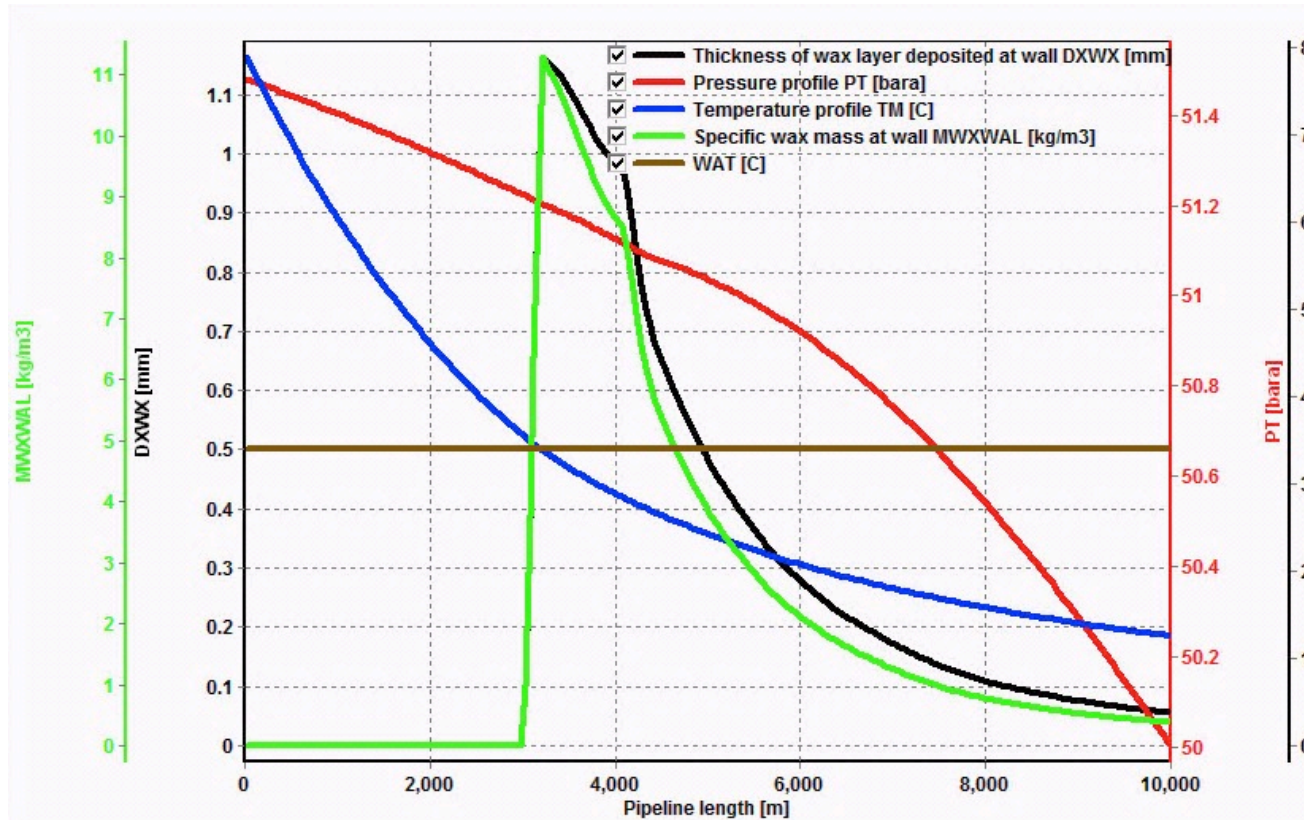


Figure 5-3 Base case wax deposition profile at 70 days simulation time

Figure 5-4 shows the wax deposition profile after 0 day, 2 days, 30 days and 70 days simulation time. Wax deposition is not recorded at the start of the simulation deduced from the 0-day thickness profile but a small thickness growth is observed after 2 days. The wax at the wall subsequently increased to 0.5mm after 30 days and to about 1.1mm after 70 days. This clearly reveals the increases in wax thickness with time.

For this flowline, if no wax control strategy is carried out, a possibility of pipe plugging is anticipated. As a rule of thumb for many subsea flowlines with a pigging control strategy, a 2mm of wax thickness is the maximum allowed wax deposition limit before the pigging is initiated[17]. The thickness curve of 1.1mm after 70 days is also consistent with the wax thickness rate observed in the wax deposition simulation of Labes-Carrier, C., et al. (2002)[15]. Additionally as the wax thickness increased, the pressure drop across the flowline increased due to the increasing oil viscosity, an increasing wall roughness and a reducing effective flow diameter in the flowline due to wax deposition.

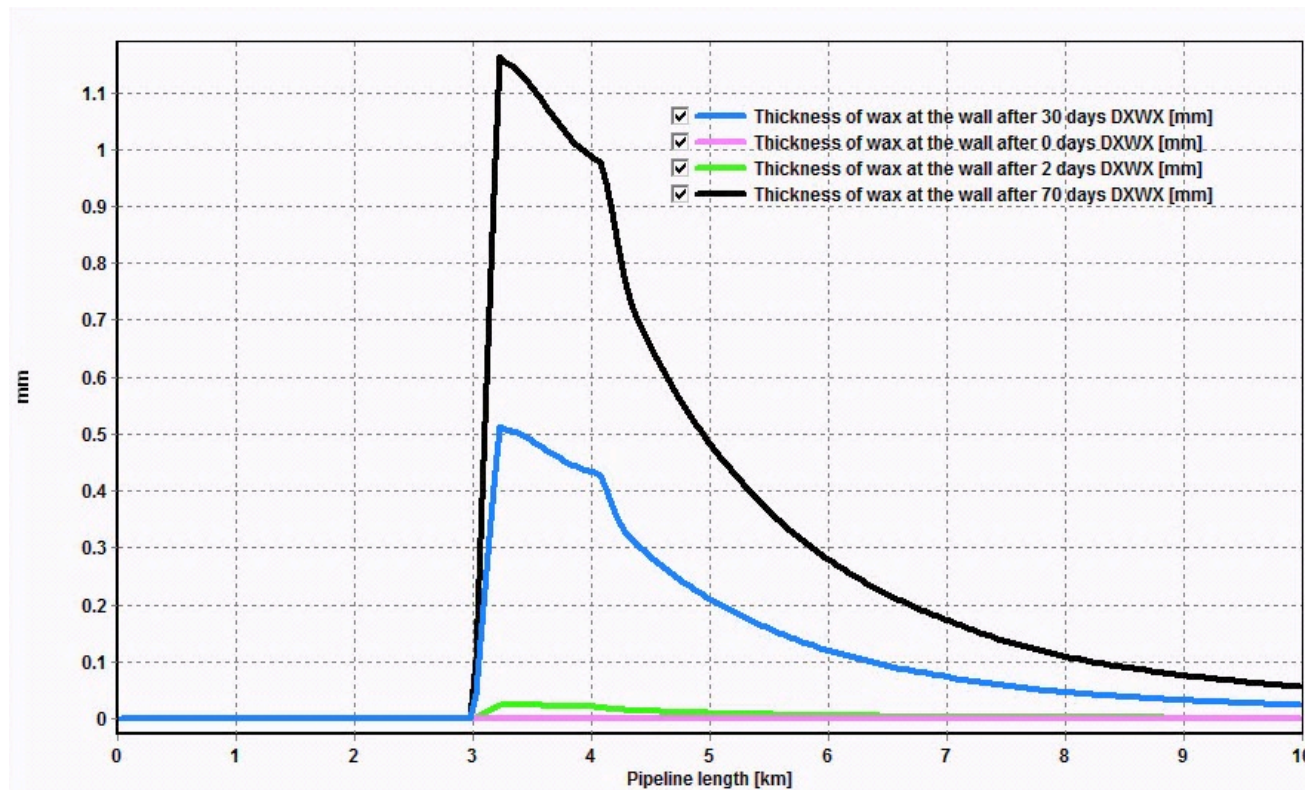


Figure 5-4 Base case wax deposition thickness with time

Taking another look at the deposition profile performance in Figure 5-5. It shows the overall heat transfer coefficient from the thermohydraulic verification properties of the flowline without wax deposition and the wax deposition simulation after 70 days respectively. Deposited wax in PIPE-4 created a sharp drop in the overall heat transfer coefficient. This deposited wax in principle creates an insulating effect to the radial heat transfer between the flowline wall and the bulk fluid, which reduces the temperature driving force, needed for wax deposition downstream the flowline. A response to this is the reducing wax thickness profile on the wall after the PIPE-4.

This observation confirms the thermal resistance property of the solid wax to the heat flow between the bulk fluid and the walls of the flowline. It also accounts for the difference in the inner wall surface temperature and the inner wall surface temperature adjusted for wax deposition observed in PIPE-4. It is notable that although deposited wax create a thermal resistance layer between the bulk fluid and inner wall in the wax deposition region, the resistance is not significant to stop the deposition process due to an available large temperature gradient existing between the flowing oil and the outer wall of the flowline.

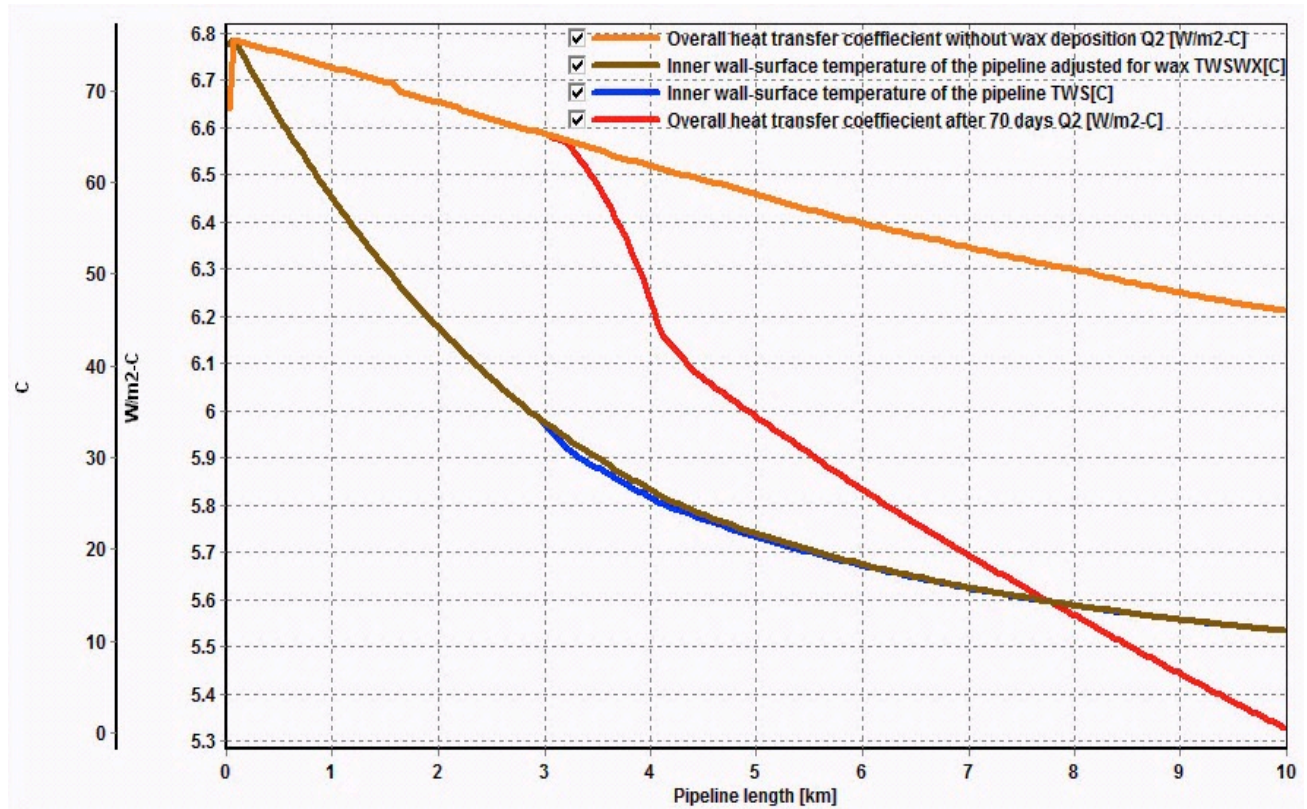


Figure 5-5 Overall heat transfer profile compared for wax deposition and without wax deposition

5.3. Annulus flowline cooling

A wax control simulation study using the cold flow concept with oil cooling to the ambient sea temperature is presented in this section. Active oil cooling at the entry of a typical well source as represented by the oil source in Figure 5-1 is created using an annulus flowline cooling configuration. The base case wax simulation in Section 5.2 is developed for controlled wax deposition. Annulus pipeline of cooling water in a typical annulus pipe in pipe flowline configuration bounds an inner pipe of carbon steel with flowing oil. The geometry of Figure 5-1 is updated to consist of a 3km annulus pipeline integrated on PIPE-1, PIPE-2 and PIPE-3. The annulus geometry is defined by a combination of the first three process pipelines in the system each of a 1km length. Tabulated geometry input in the annulus is given in Table 5-6.

Table 5-6 Annulus flowline geometry

Pipe	X	y	Length	Elevation	Section	Diameter
	[m]	[m]	[m]	[m]		[m]
Start Point	0	-100				
PIPE-1	1000	-100	1000	0	20	0.2032
PIPE-2	1000	-100	1000	0	20	0.2032
PIPE-3	1000	-100	1000	0	20	0.2032

The geometry of the annulus is spanned such that sufficient cooling fluid by seawater at a temperature of 6°C exchanges heat with the hot oil through the walls of the inner pipeline thereby creating a wax deposition zone in the oil flowline. A co-current or counter current water flow configuration can be selected for the oil cooling. Both flow configurations are investigated in this wax deposition model.

Figure 5-6 and Figure 5-7 shows the schematic representation of the annulus configuration. It shows the oil source into the oil flowline, the annulus flowline of 3km length and an additional 7km combination of the oil flowline. Cooling water flow direction into the annulus-cooling region is represented as seawater flowing in either of co-current or counter current direction by flow arrows. A created wax deposition zone in the annulus region is indicated. Wax free oil flowing at the temperature of the surrounding environment is expected after the annulus.

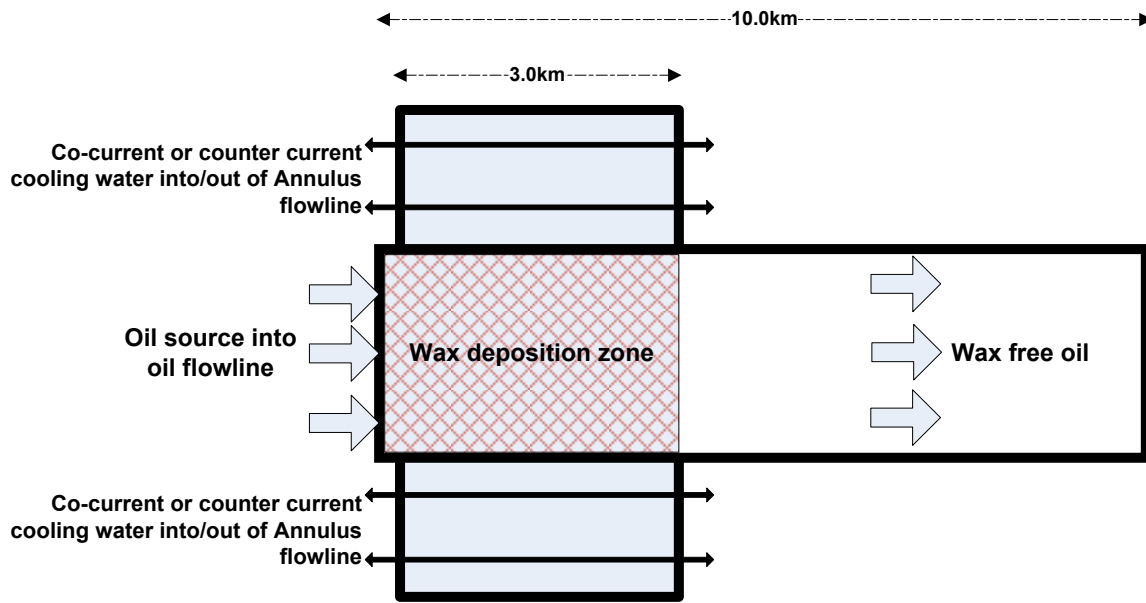


Figure 5-6 Annulus integration in the pipe line

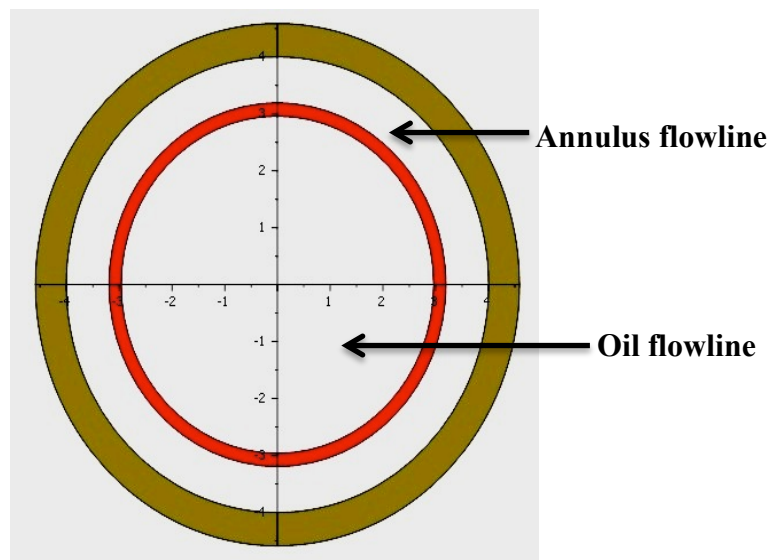


Figure 5-7 Annulus combination for flowline cooling (front/end view)

The outer pipe of the annulus combination is made of carbon steel material with a subsea soil layer in contact with the steel wall replicating typical subsea soil environment. The annulus heat transfer properties is defined with a initial heat transfer coefficient of $60\text{W/m}^2\text{-C}$ on the inner wall of the annulus pipe and a non-insulated outer wall with an ambient heat transfer coefficient of about $200\text{W/m}^2\text{-C}$ supplied from OLGA properties. Cumulative overall heat transfer coefficient of about $7.4\text{W/m}^2\text{-C}$ is obtained from OLGA for the annulus pipe in pipe system. More wall properties of the annulus and simulation inputs are given in Table 5-7 and Table 5-8 respectively.

Table 5-7 Pipe Materials for Water- Annulus Flowline

	Thickness	Conductivity	Density	Heat Capacity
	[m]	[W/m-k]	Kg/m ³	J/Kg-k]
Carbon Steel	0.2362	45	7850	470
Subsea sandy soil	0.0025	0.3	1300	1410

Table 5-8 Simulation input for the annulus configuration

Parameter	Value
Annulus length	3km
Cooling fluid	Sea water
Cooling water temperature	6°C
Cooling water mass flow rate	58kg/s
Cooling water velocity	4.8m/s
Wax deposition	ON (wax model ~ RRR)

5.3.1. Co-current flowline cooling

The base case model is updated for a co-current cooling simulation. The co-current cooling case named co-current cooling case Case A is simulated for a 70-day time. It is observed that terms used in describing two fluid flows in the same direction include parallel flow, co-current flow or concurrent flow. In this work co-current has been used for all cases representing flows of fluid in the same direction.

The oil with fluid composition listed in Table 4-1 flowing at a standard flow rate of 500Sm³/day through the oil flowline is cooled by a co-current flowing water typically sea water at a temperature of 6°C in the annulus path as described in Section 5.3 above. OLGA schematic representation of the co-current annulus cooling is shown by Figure 5-8. Expected outlet temperature of the oil from the annulus region is the temperature of the cooling water exiting the annulus.

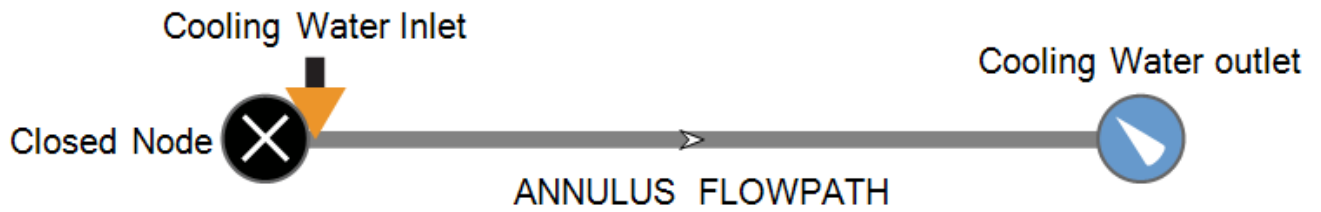


Figure 5-8 Co-current cooling path in an annulus configuration

Figure 5-9 shows the profile plot of the annulus cooling water temperature and the oil temperature as well as the wax deposition thickness in the oil flowline. Further drop in the temperature of the oil to ambient seawater is observed in the temperature plot after the annulus-cooling zone. This is expected as the oil flowline transfers heat from the bulk oil to ambient sea because of the good heat conduction property of the carbon Steel.

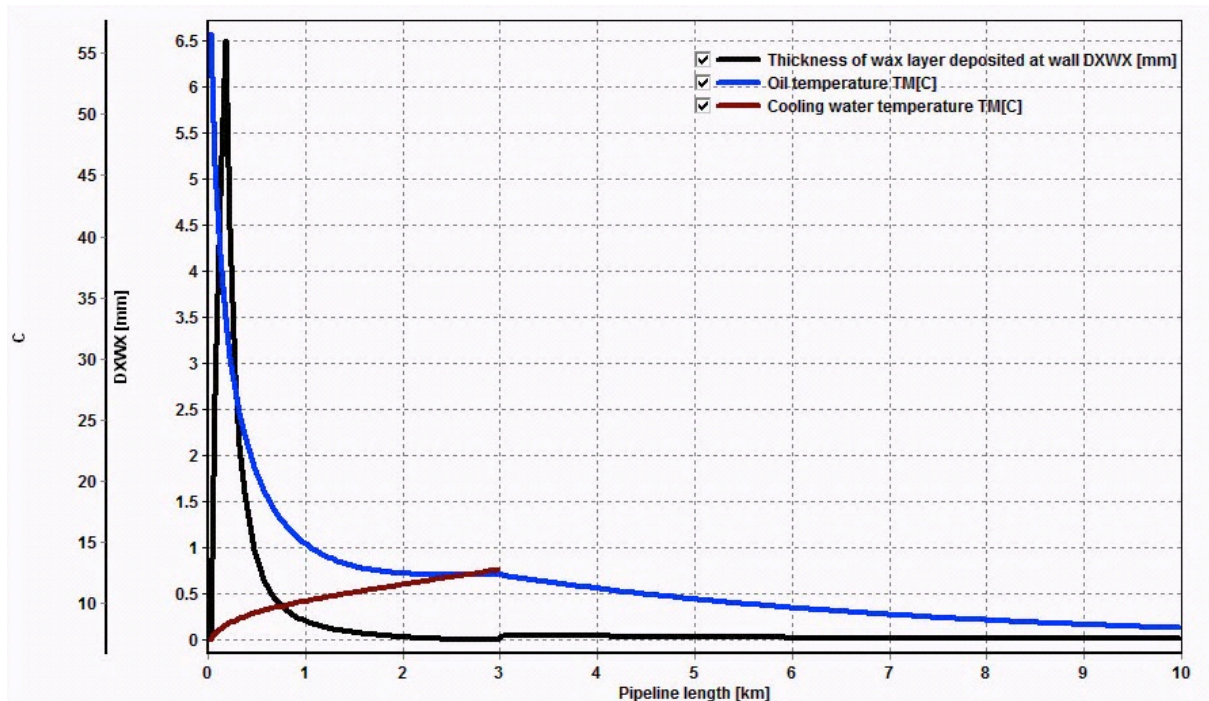


Figure 5-9 Wax thickness profile at the wall after annulus cooling of 70days at 500Sm³/day

A combination of a more developed annulus cooling configuration can further be implemented for the wax deposition zone, but the simplistic model of this thesis is made to confirm the prospects of the annulus cooling concept as an effective wax control technology in subsea flowlines.

Cooling through the annulus thrives on the surface area available for heat transfer, the heat transfer properties of the annulus materials and the heat exchanges between the walls of the annulus flowline and the oil flowline.

For this case with oil flow rate of $500\text{Sm}^3/\text{day}$, wax deposition started at the immediate inlet of the wax deposition zone where the temperature gradient is greatest. This temperature gradient in PIPE-1 provides a large driving force for heat transfer between the oil and the cooling water. A wax thickness of 6.5mm is deposited in this pipe, however the wax thickness gradually reduces as the temperature gradient diminishes through the annulus.

The temperature profile of the cooling water and oil is depicted in Figure 5-9. The profile performance of the temperatures between the cooling water and oil reveals a decaying temperature difference as the fluid passes the annulus. The temperature difference approaches zero at PIPE-3 resulting in a near equal exit temperature of about 12.74°C for both fluids from the deposition zone.

As illustrated in Figure 5-6 using the annulus cooling concept, the wax deposition zone is the anticipated effective wax deposition region where all potential wax drop out of the oil as deposited wax on the inner wall of the pipeline. A trail of wax deposition is observed out of the wax deposition zone when the oil exits the annulus. This is observed from the increases in wax thickness at the exit of PIPE-3. The effectiveness of this co-current annulus cooling to limit wax deposition to the wax deposition zone is doubted.

A co-current cooling Case B with a increased oil flow rate of $5000\text{Sm}^3/\text{day}$ is simulated for parameter analysis and to test the consistency of wax deposition in the wax deposition zone. The wax thickness profile and cooling performance is presented in Figure 5-10.

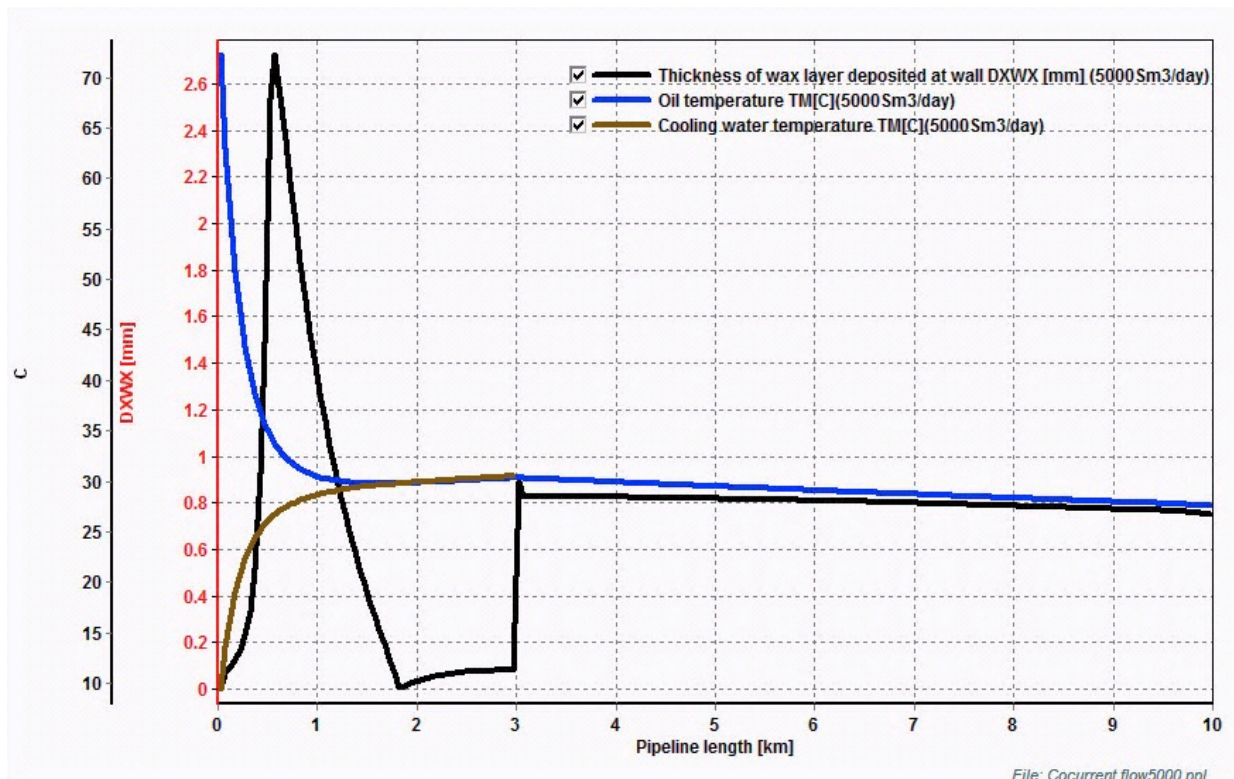


Figure 5-10 Wax thickness profile at the wall after annulus cooling of 70 days at 5000Sm³/day

For this increase, exiting temperature of both cooling water and the oil out of the annulus region rises to 30.37°C as compared to exiting temperature of 12.74°C in the co-current cooling of Case A. A difference of about 1°C exist between the WAT and the temperature of both fluids exiting the annulus region. The net effect of the high exit temperature is a reduced temperature driving potential sufficient to induce wax deposition for all components in the flowing oil in the wax deposition zone. A consequence of this is a large deposition of wax on the oil flowline after the annulus.

Wax is not fully taken out of the oil in the wax deposition zone caused by two reasons. First the limited temperature difference between the cooling water and the flowing oil and secondly, the low temperature driving potential between the WAT and the temperature of the flowing streams. An alternative process choice for this co-current case is to increase flow rate of the cooling water to match the cooling requirement of the oil such that the cooling water temperature is substantial below the wax appearance temperature in the wax deposition zone with the aim of preventing downstream deposition of the wax after the wax deposition zone.

5.3.2. Counter current flowline cooling

The base case model is updated for counter current cooling named counter current cooling Case A. The counter current cooling Case A is simulated for a simulation time of 70days with case input properties similar to the co-current cooling Case A. Oil through the flowline with composition given in Table 4-1 is cooled in the annulus region of the flowline. Cooling water supplied into the Annulus flowline at 6°C in PIPE-3 Section-20 flows counter currently against the oil in the oil line as shown in Figure 5-11. The annulus line consists of a pressure node at the cooling water outlet as well as a closed node without mass and energy interactions illustrated by Figure 5-11.

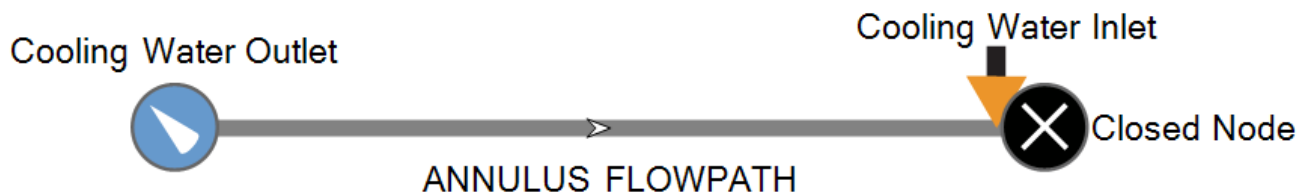


Figure 5-11 Counter-current cooling path in an annulus configuration

The result obtained for the wax deposition simulation in Figure 5-12 shows the temperature profile of the cooling water, the oil and the wax deposition thickness in the oil flowline for oil standard flow rate of 500Sm³/day. Unlike the co-current cooling case with a continuous temperature drop after the annulus, observed exit temperature of the oil from the annulus section is the inlet temperature of the cooling water of 6°C. Exiting oil temperature from the annulus is at the ambient temperature therefore no temperature gradient exist between the oil and the ambient sea water for this counter current flow model.

Potential wax deposition downstream the annulus is avoided as all-potential wax drop out in the wax deposition zone within the annulus region. In this model, the wax deposition zone much more performs as the anticipated effective wax deposition region where all potential solid drop out of the oil as wax on the wall of the flowline.

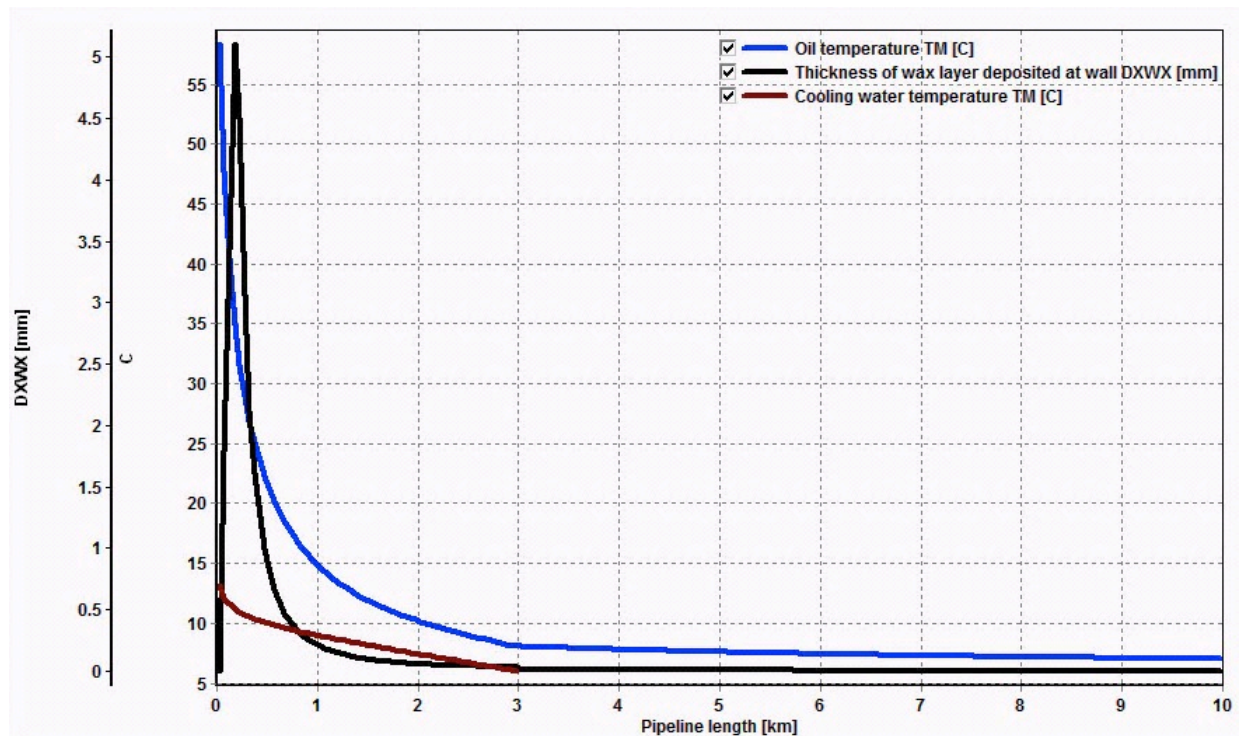


Figure 5-12 Counter current wax thickness at the wall after annulus cooling of 70days

As observed in Figure 5-12, a lower wax deposition thickness of 5mm is seen in the immediate inlet of the wax deposition zone when compared with a wax thickness of 6.5mm of the co-current cooling Case A at same flow rate. The low value of wax thickness in this counter current flow is attributed to a lower temperature driving force at the inlet of the wax deposition zone in this counter current model.

The temperature profile in Figure 5-12 clearly shows a relatively consistent temperature difference existing between the cooling water and the oil through the wax deposition zone. This provides a better cooling performance and as such eliminates possible trail of wax deposition downstream the oil flowline outside the wax deposition zone.

A counter current Case B for a parameter analysis to determine the effect of an increase in the standard flow rate of oil is performed similar to the co-current model. Profile result for the wax thickness and the temperature of the two fluids in the wax deposition zone for oil flow rate at $5000\text{Sm}^3/\text{day}$ is presented by Figure 5-13.

A uniform temperature difference that provides for an even driving force exists between the cooling water and the flowline. This offers a better temperature driving potential needed to induce wax deposition through the wax deposition zone.

After the annulus, wax free oil is transported through the oil flowline, as there is no temperature gradient available for wax deposition at oil temperatures below the WAT. Deposition downstream the oil flowline is therefore eliminated.

Also observed is the increase in wax deposition area within the wax deposition zone as compared to the simulation observation of the counter current Case A in Figure 5-12. Though a lower wax thickness of about 3.7mm is deposited on the walls but a more consistent filling of the wax is observed and more volume of wax is precipitated and deposited in the wax deposition zone

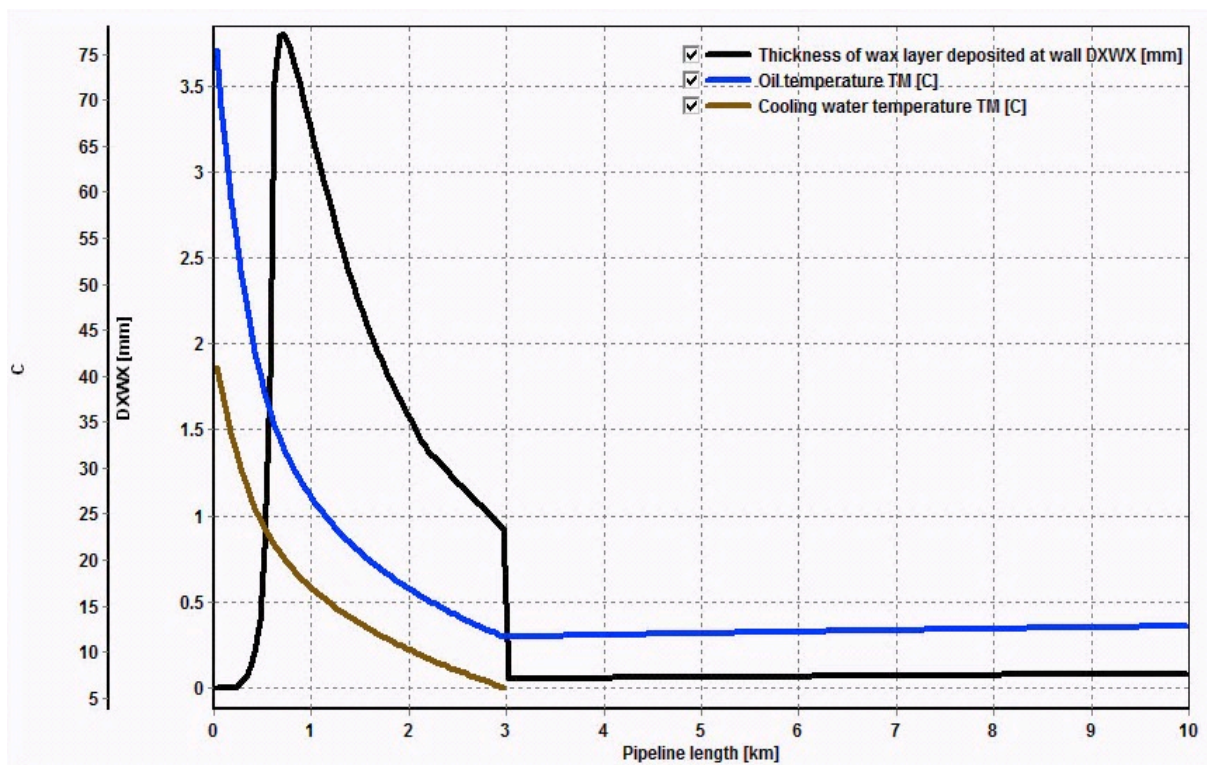


Figure 5-13 Counter current wax thickness after annulus cooling for 70days at increased oil rate

This wax control strategy that ensures wax are deposited only in a wax deposition zone as illustrated in Figure 5-13 provides an important wax control approach in subsea flowline pigging where mechanical pigging of wax is implemented as a wax control technology. It provides an economic approach in maintaining pigs such that only wax deposition zone are pigged. This would reduce pig residence time, pigging lengths and overall pigging cost. Additionally, the accuracy of wax thickness necessary for pigging criteria in subsea flowlines can be accurately quantified with higher degree of reliability in the wax deposition zone.

As discussed for Figure 5-13, deposition volume in the wax deposition zone increased significantly for the counter current Case B of the counter current cooling simulation. This deposition does not sufficiently fill or plug the annulus as projected.

Based on PVTsim solubility analysis of Figure 4-2, at an operating pressure of 100bar, the weight of wax out of solution increases to about 6% at 10°C. A continued increase in the wax weight percent is predicted as the oil temperature drops based on the solubility curve. With this in mind, 6% weight of deposited wax is anticipated in the wax deposition zone for the simulations predictions of OLGA at 10°C temperature, but this is not so. A careful look at the mass balance for wax prediction in the counter current Case B simulation case reveals that a considerable fraction of the precipitated wax is transported through the oil flowline in the oil as wax dispersed in oil and as suspended wax in oil. This is clearly shown in Figure 5-14.

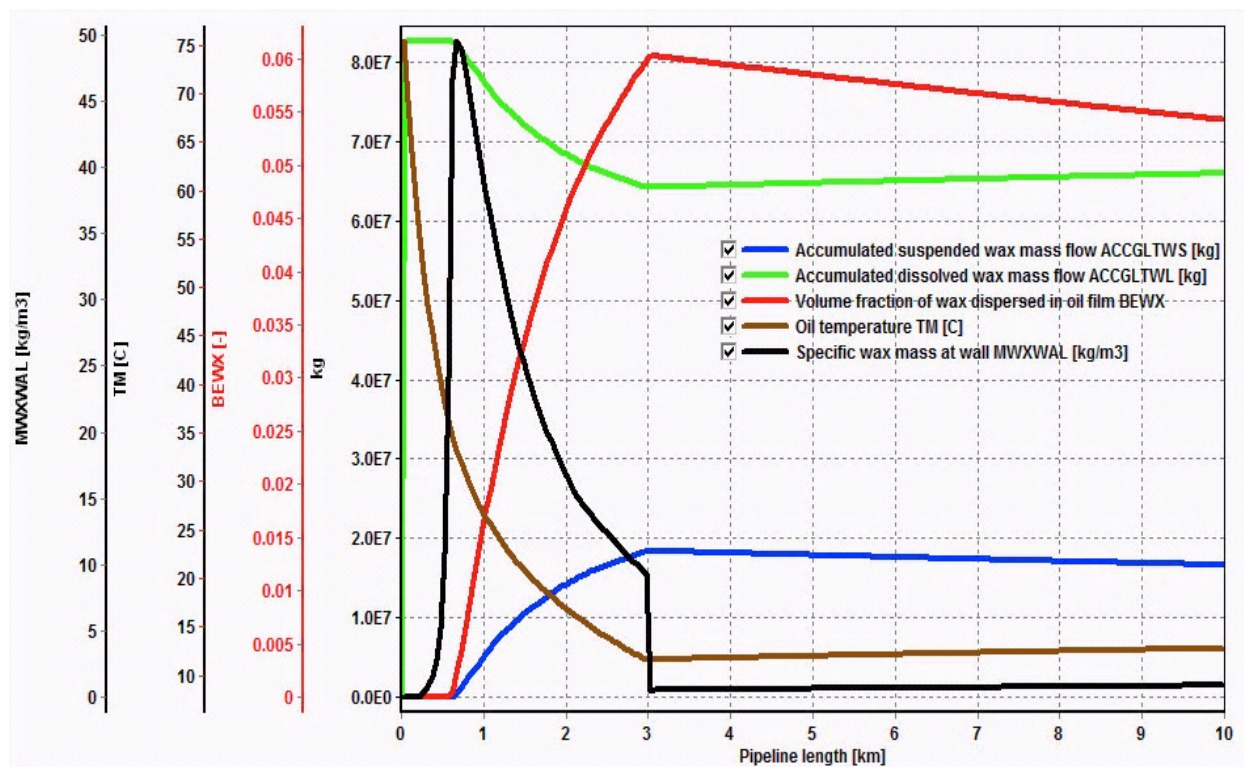


Figure 5-14 Mass balance of precipitated wax in the oil flowline after 70days simulation

Figure 5-14 shows about 6% of precipitated wax is dispersed after the annulus at 10°C. This precipitated wax percent agrees with the 6% weight % precipitated wax from PVTsim at same temperature. Some fraction of wax is also dissolved in the oil and does not precipitate out of solution. The dispersion effect is seen to reduce the specific wax mass on the wall in the wax deposition zone and as a consequence, the deposition process does not block the wax deposition zone.

These dispersed and the suspended wax acts an important transport form of stable wax solid downstream the flowline and it provides a careful control wax transport mechanism to managed precipitating and depositing wax in the flowing oil. The dispersed and suspended wax solid is suggested to be produced when loosening case is simulated. Vicious forces and operating flow conditions are also considered to contribute in influencing the magnitude of the dispersed and the suspended wax in the oil. A combination of the dispersed wax, suspended wax, the deposited wax and wax dissolved in the oil make up the total balance for the weight % of wax in the flowline.

5.4. Wax Liberation Simulation

Methods and model to loose out deposited wax from the wax deposition zone is investigated and presented. Heating of the pipeline is provided by hot water exchanging heat with the outer wall of the oil flowline through the annulus configuration.

Reported experimental observations from the Statoil Porsgrunn flow loop suggests that a co-current or counter current heating through an annulus configuration would release stable wax into the oil from an initial wax deposit on a flowline wall[19]. After an initial cooling to deposit wax in the wax deposition zone, a counter current heating water is passed through the annulus flowline in this model. Wax release from wax deposition zone is illustrated by Figure 5-15 and Figure 5-16.

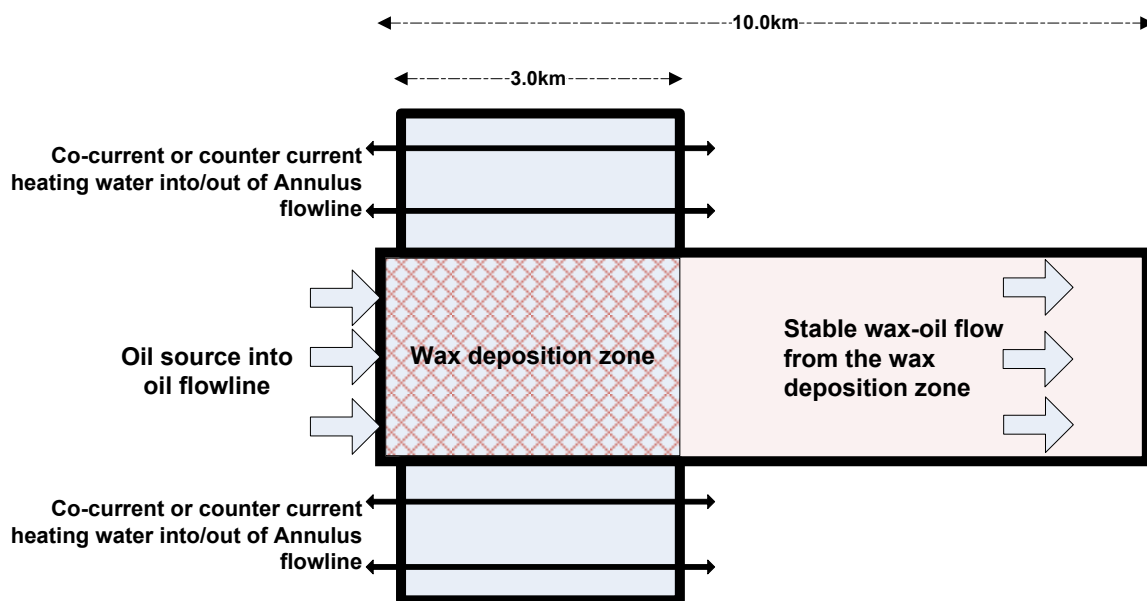


Figure 5-15 Stabilized wax liberated from annulus in the wax deposition zone

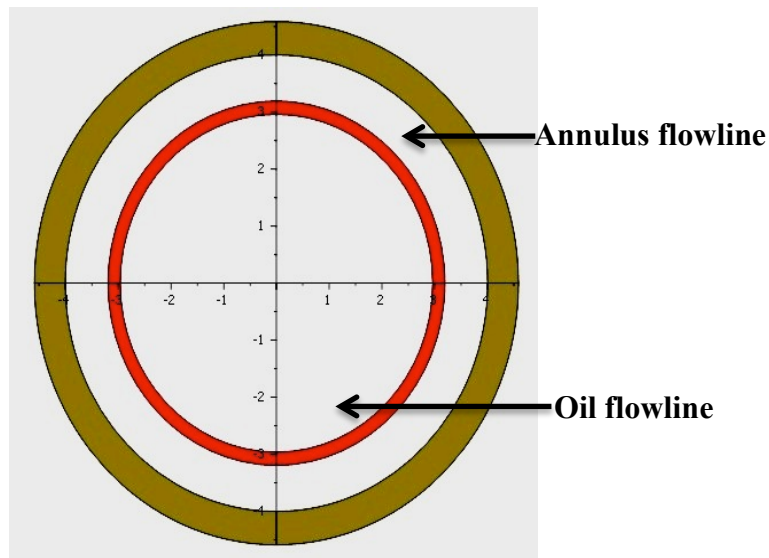


Figure 5-16 Annulus combination for wax liberation

Counter current flowing hot water through the annulus is simulated in OLGA to loosen the deposited wax obtained from the counter current cooling Case B simulation of Section 5.3.2 in the wax deposition zone. The representation of the annulus heating through the annulus flow path in OLGA is shown by Figure 5-17.

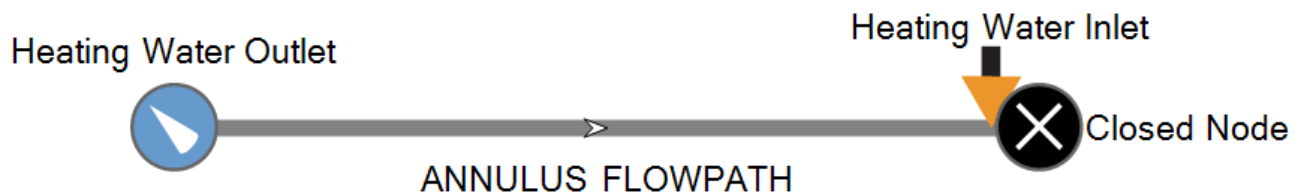


Figure 5-17 Counter-current heating path in an annulus configuration

Particular emphasis is made to avoid melting the deposited wax. The heating strategy is selected such that the heating sufficiently liberates the wax but does not melt the wax. The heating period is selected to be less than the deposition period based on the experimental suggestion from Porsgrunn flow loop[19]. Additionally, the heating water temperature and temperature of the inner wall in the wax deposition zone is selected to be less than the wax dissolution temperature to avoid melting the wax. As a rule of thumb derived by real field experiences, the wax dissolution temperature in oil and gas pipeline is about 20°C higher than the wax appearance temperature[17]. Selected temperature of the heating water is taken to be above the wax appearance temperature to avoid any further precipitation of wax out of the oil.

For this wax liberation model, oil flowing at 5000Sm³/day at an inlet temperature of 80°C flows into the oil flowline through the wax deposition zone while an additional hot water flows counter currently through the annulus flowline. A restart file case created from the counter current cooling Case B wax deposition simulation of Section 5.3.2 is updated for the wax loosening simulation. The hot water is set at 35°C.

As obtained from PVTsim, the oil has a WAT of 32°C and consequently a dissolution temperature of 52°C as indicated in Table 5-9. A temperature difference of 3°C exists between the heating water and the WAT while a temperature difference of 17°C exist between the wax dissolution temperature and this loosening temperature. Anticipated heat exchange occurs between the outer wall of the inner pipe and the heating water flowing in the annulus.

Table 5-9 Temperature characteristic of flowing streams

Oil Inlet Temperature	80°C
Hot Water Temperature	35°C
Oil WAT	32°C.
Expected Oil WDT	52°C

Alongside the wax loosening simulation, consideration is given to determine the effect of the wax dissolution option available in the RRR model on the wax loosening simulation results. Figure 5-18 shows the initial wax deposition thickness in the wax deposition zone before hot water heating, the wax thickness after a heating time of 50 days, the wax thickness after a heating time of 50 days when the dissolution option is activated and the temperature profiles of the flowing streams in the annulus and the oil flowline.

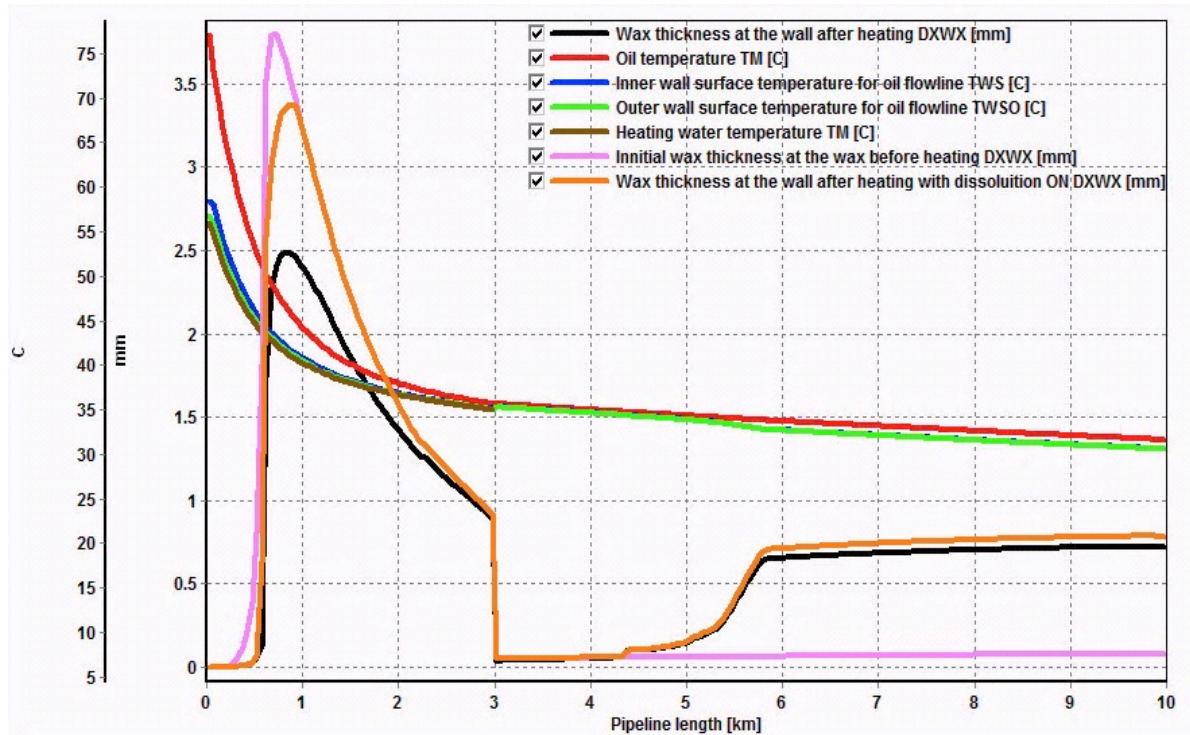


Figure 5-18 Wax thickness profile for a counter current heating configuration after 50 days

Figure 5-18 result further indicate a temperature difference of 3.1°C between the inner wall of the oil flowline and outer wall in contact with the hot water of the wax deposition zone at the onset of heating in PIPE-1 and a temperature difference of 0.1°C at the exit of the wax deposition zone. A combination of the hot oil and the hot water through the annulus heats up the inner wall in contact with the deposited wax in the wax deposition zone. The hot oil provided the significant heating contribution in PIPE-1 of the wax deposition zone where wax thickness is greatest while the counter current hot water maintains the heating of the wax deposition zone downstream the annulus.

Results of simulations compared for the effect of wax dissolution shows that higher wax is released from the wall when the dissolution option is ignored and therefore better loosening capability for wax at the wall when wax dissolution is ignored. This wisely suggests that for a release of deposited wax, wax dissolution conditions of the oil must be avoided.

The lower loosening performance of the loosening simulation case with a dissolution option is also believed to signify the properties of the model implemented in OLGA. As recorded in Section 2.2.1, the RRR implements a dissolution model that calculates to melt solid wax along the flow profile based on the solubility curves criteria supplied from the PVT file obtained at a user supplied wax

dissolution pressure. The OLGA dissolution model in effect will calculate for the wax melting properties based on solubility temperatures of the wax at a given pressure.

The effective melting calculation in the OLGA model explains the re-deposition observation of wax downstream the flowline in Figure 5-18. The sum of removed wax at the wall goes into the bulk oil as re-dissolved wax, as suspended wax and wax dispersed in the oil. After the annulus heating, the oil temperature drops below the WAT; re-dissolved wax is re-precipitated out of the bulk oil and thereafter re-deposited on the walls of the oil flowline.

An efficient loosening of the wax would release out the wax from the walls of the wax deposition zone as stable flake-like wax crystals. Released stable wax will mix with the oil by natural convection while fluid forces will transport the wax in the oil through the downstream flow. The re-deposition of wax downstream the flow encountered in this loosening model reveals the inability that OLGA could not accurately handle the models for the loosening of released solid wax. It presents a gap in process modelling of wax in process simulator as much as it reveals a technology gap in wax control technologies.

Released wax is believed to be transferred in the bulk fluid as dispersed or suspended wax by fluid forces. Of thoughtful concern is the stability of dispersed or suspended wax released by the heating process into the bulk fluid. The stability of the wax is expected to depend on the form and structure of the wax released in to the oil as well as the operating conditions of the flowline.

Figure 5-18 provides no indication on the morphology of liberated wax. Deduction from Figure 5-14 indicates that wax in the system would be dissolved, suspended or dispersed in the oil. Crystal stable dispersion of the wax is expected to nucleate more stable dispersed wax and avoid re-dissolving in the oil. The ability of the model to generate crystal stable flakes of released wax and its ability to nucleate more wax flakes in the dispersed form of the wax phase is unavailable.

Experimental reports by University of Utah records that wax precipitates are nucleated in cold flow equipment and the presence of these precipitated wax decreased the tendency of wax crystals deposition downstream the flow[22]. This is schematically illustrated by Figure 5-19. Stable crystal of precipitated wax transported in the cold stream is suggested. The challenge with this model is that the effect of heat and mass transfer and surface-solid deposition in the cold flow equipment is thought to be negligible. The question about wax deposition in this cold flow equipment remains unclear and unanswered since deposition of precipitated wax would be a resulting consequence of the

wax concentration difference and thermal gradient in the cold flow equipment which is always present as flowline operating condition in a subsea environment.

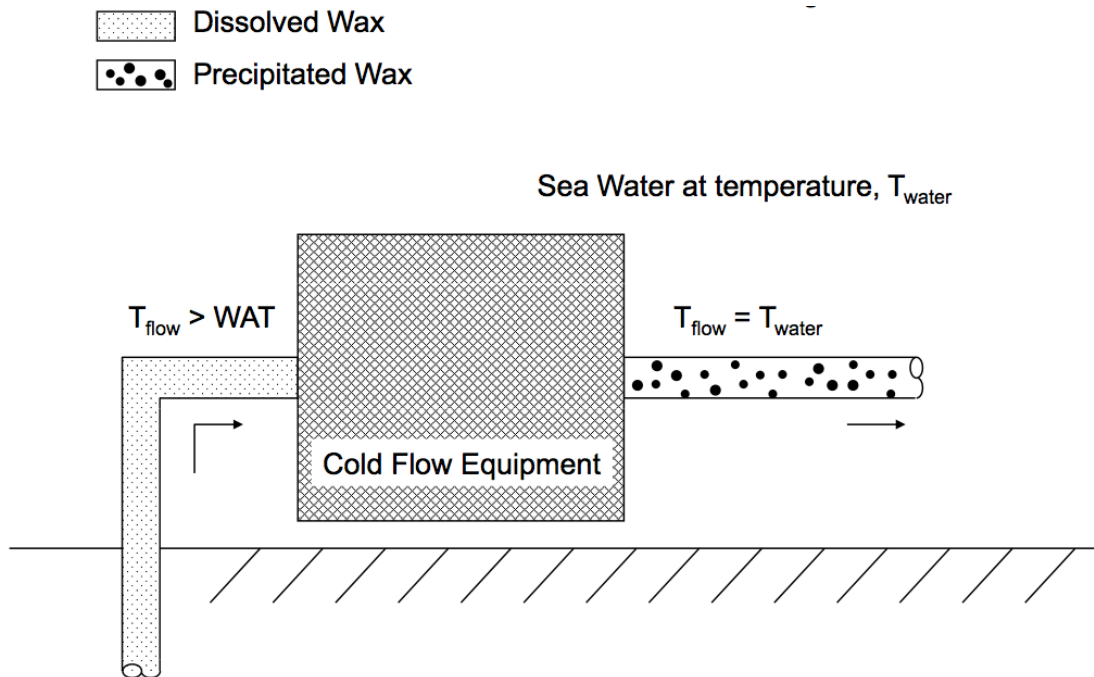


Figure 5-19 Cold seeding concept in a Cold Flow Equipment[41]

The experimental report by University of Utah further records a seeding of wax in a nucleation zone through an injected polyethylene pellets[22]. It observes a significant reduction in the deposition rate but there are arguments about the seeding temperature, effect of the polyethylene pellets acting as crystal modifiers or as nucleation sites on the morphology of precipitated wax. If the latter is justified, then the polyethylene pellets can be considered as wax modifiers that will in principle reduce or eliminate wax deposition. The success of the polyethylene pellets to reduce or eliminate deposition is yet to be recorded; it is assumed that adding the polyethylene pellets will not eliminate the wax deposition challenge - the primary reason for a wax control strategy.

6. A Proposed Cold Flow Wax Control Concept

This proposed wax cold flow concept is a combination of an annulus cooling concept for the active cooling of the oil to sea temperature in an attempt to initiate wax deposition in a wax deposition zone as presented in Section 5.3, an annulus heating of the walls of the wax deposition zone to release stable wax from the walls of the wax deposition zone based on the experimental records from the Statoil Porsgrunn flow loop and a wax liberation model using active fluid forces to generate effective wax stripping in the wax deposition zone.

As demonstrated with the counter current annulus cooling in Section 5.3.2, sufficient oil cooling to sea temperatures in a designed wax deposition zone would induce potential wax deposition in the wax deposition zone without further deposition after the zone. This is observed from the simulation results of Figure 5-13.

The controlled deposition in a wax deposition zone is further developed to consist of wax liberation using induced stripping forces and minimum heating of the inner wall of the wax deposition zone to liberate stable wax from the wax deposit at the walls of the wax deposition zone as illustrated in Figure 6-1 and Figure 6-2 using an annulus flowline combination for wax deposition zone wall heating.

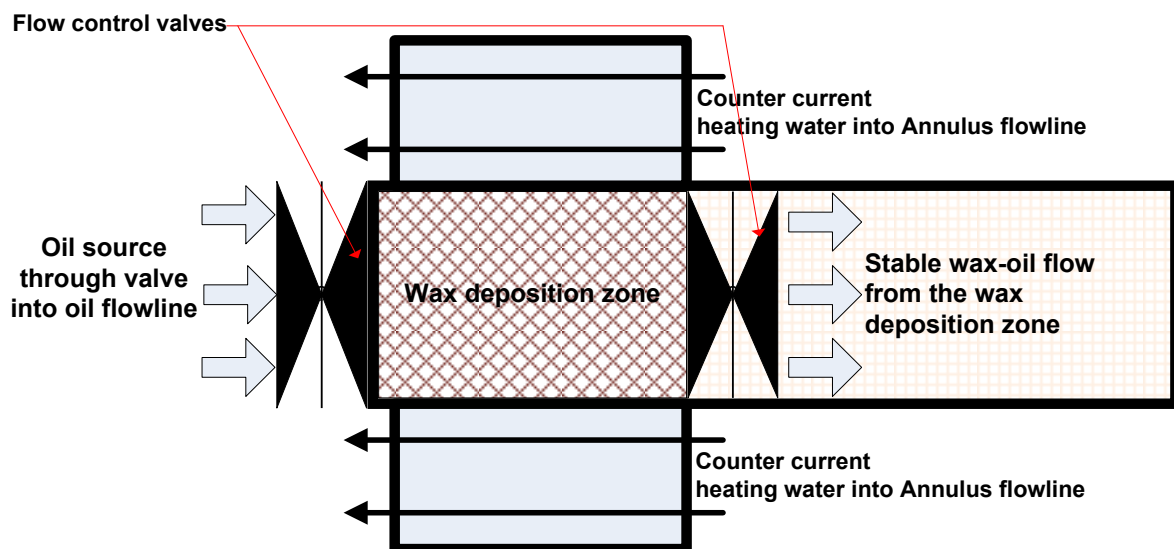


Figure 6-1 Wax liberation concept with flow control valves

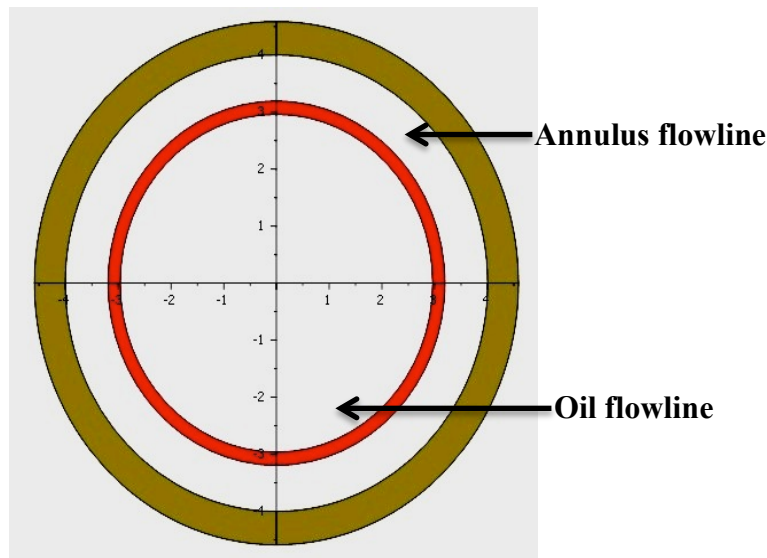


Figure 6-2 Annulus combination for wax liberation

This wax liberation concept depends on active control of fluid force to generate a stripping effect on the wax on the wall. Pressure regulating valves installed at the inlet and exit of the wax deposition zone control fluid velocity, fluid pressure and there by regulates flow turbulence in the wax deposition zone. Fluid power can be maximised within the controlled deposition zone to generate sufficient stripping power needed to slough off stabilised wax pieces from the walls of the wax deposition zone.

Counter heating of the inner walls of the flowline to increase the effectiveness of liberated wax can be additional provided through the annulus flowline as illustrated in Figure 6-3. At temperatures less than the wax dissolution temperature, stripping and liberation of the wax due to heating of the walls of the wax deposition zone will be generated from the deposited wax into the flowing oil, which is transferred as stable crystals or pieces wax flakes downstream the flowline.

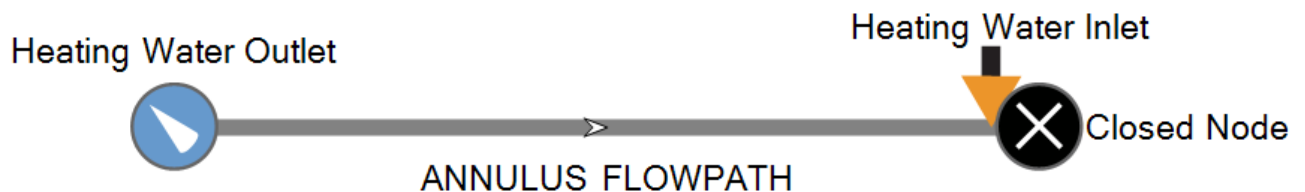


Figure 6-3 Counter current heating path through an annulus flowline configuration

A combination of the wax stripping potential and the wax heating potential permits minimum heating of the wax deposition zone below the wax appearance temperature. At supplied heating temperatures

below the wax appearance temperature, wax precipitation continues in the wax deposition region and effectively continuous wax deposition is produced in the zone. This ensure a continuous depletion of wax from the bulk fluid within the wax deposition zone at every operating time in the system as opposed to a annulus heating without a wax stripping strategy where necessary heating temperatures of the inner walls of the wax deposition is above the WAT for sufficient wax releases from the wall.

The sloughing of stable crystals from the wall line using fluid stripping force further provides the possibility to supply heating only at peak conditions of wax deposition and eliminates for a continuous heating requirement at all period of wax liberation.

7. Conclusion

The major aim of this thesis is to develop models for wax control in oil and gas production system. Emphasis was given to investigate the reliability of available process simulator in modelling new strategy of wax control in oil-dominated system. Wax deposition mechanisms, models of wax deposition for predicting wax deposition and thermodynamic models that evaluate wax precipitation are investigated. Wax deposition simulation is carried out with the PVTsim package and OLGA wax module simulator. An annulus active cooling model and an annulus heating model for wax control is developed.

Molecular diffusion and Shear dispersion are the primary wax deposition mechanisms, the effect of Gravity settling, Soret diffusion, and Shear stripping are fairly insignificant. Molecular diffusion and Shear dispersion mechanisms are the considered mechanisms in the OLGA simulator used for the wax control simulation in this thesis. There exist a need for a robust model that incorporates all potential mechanism to eliminate deposition mechanism uncertainties as the effect of shear stripping is considered to be significant in high velocity flows. The Singh et al (2000) wax deposition model is a distinguished model that considers internal diffusion between molecules of deposited wax layers, it accounts for aging and gelling in wax deposition.

The Pedersen (1995) wax model incorporated with cubic equation of state is selected for the thermodynamic analysis used in this thesis work. Its equilibrium calculation of wax forming and non-wax forming fractions as wells as the calculation of the equation of state critical properties present a consistent model for the equilibrium prediction of precipitation wax in oil and gas mixtures. The Predictive Uniquac thermodynamic for the local interactions between like and unlike solid interactions as well as solid –liquid interactions in a wax oil mixture affords a more reliable representation of thermodynamic interaction of wax-oil solutions. It justifies and accounts for wax phase transitions and non-ideality present in thermodynamic interactions of wax oil mixtures.

From the wax control simulation performed in OLGA, it is shown that the annulus cooling model can provides for an effective strategy to deposit wax in an intended wax control zone called the wax deposition zone in an oil and gas subsea flowline. The transport of oil at ambient sea condition eliminated the needed temperature-driving force for wax deposition after the wax deposition zone. The deposition in a wax deposition zone eliminated downstream deposition and offers free wax transport of oil in subsea flowlines.

A wax-loosening model for deposited wax within a wax deposition zone is developed in OLGA using the annulus hot water heating model. Model results produced initial release from the wax wall but insufficient to liberate all wax at the wall. A further re-deposition of wax is observed downstream the flowline. Result confirms the incapability of the OLGA process simulator to reliably produce experimental observation of released wax from the wall surfaces. The simulation results further emphasize the need for a reliable wax control model in public process simulator available in the oil and gas industry

A wax cold flow control model using induced fluid stripping forces and minimum heating of the wax deposition zone is proposed. It presents the possibilities to maximise contributing stripping power of fluid forces and a minimum heating through annulus heating path to slough pieces of crystal stable wax, transported downstream at ambient temperature of a subsea flowline. It also affords an unstopped deposition of wax in a wax deposition zone by providing heating when needed at temperatures below the wax appearance temperature.

8. Further Work and Recommendations

Foremost, a simplified cooling approach is designed for the annulus-cooling configuration developed in this thesis; an extended further analysis is essential to determine the cooling performance of the co-current and the counter current cooling configuration in a more advanced or rigorous cooling configuration.

As confirmed from this work, the counter current cooling configuration provides better cooling performance than the co-current cooling configuration at the same operating condition but advanced cooling models could be tested involving integrated cooling sources and outlets on the annulus. A combination of installed counter heat exchangers on the oil flowline could also provide more rigorous cooling performance and hence better efficiency of deposition within the wax deposition zone. Process variables that need to be optimised is the length of the annulus and the flow rate of cooling water based on the overall heat transfer coefficient of selected cooling configuration.

For a wax loosening model, development of controller systems for the controlled heating of subsea flow lines implemented alongside the annulus configuration should also be investigated. In real field systems, automated heating systems should be activated or deactivated based on designed wax thickness limit supplied into automated controllers. This activates the heating systems when wax is fully deposited in the wax deposition zone and deactivates the heating systems when the wax is loosened from the wall as supplied into the desired controller configuration.

Further experimental work to determine concentration of stable wax released with temperature in an annulus heating flow loop is needful. The development of the loosening model can be implemented employing the concept used for the tuning of wax precipitation based on wax solubility observation when oil is cooled at various temperatures as implemented in PVTsim.

Measurement of stable wax released can be recorded when walls of an annulus flowline configuration is heated in an experimental flow loop at desired temperatures. Care should be given to the heating such that the heating temperature is always below the wax dissolution temperature such that $WDT < WLT < WAT$ where WDT , WLT and WAT is wax dissolution temperature, wax loosening temperature and wax appearance temperature respectively.

Concentration of stable wax in the oil at selected temperatures should be analysed, which will in turn provide information about loosening tendencies and stability of the waxes with respect to heating and wax heating period. Observation from wax released at various measured temperature can be

developed into a mathematical model for the calculation of wax loosening characteristics of wax deposition on pipe walls in process simulators.

A challenge to this envisaged suggestion is the need to measure loosening tendencies of different oil before a general correlation can be effected. It is therefore important that experimental loosening correlations should include fluid compositional parameters before generalised loosening correlations can be accurate.

Experimental verification of the stripping potential using active and induced fluid forces in the proposed cold flow wax control concept of Section 6 is needful. Optimised configuration of flow control valves and pressure control at the inlet and outlet of the wax deposition zone is required. More also, particle size measurement and the morphology of released stable crystals of wax from the cold flow liberation models need to be determined. The aggregate structure of wax flakes that promotes the stability of liberated wax crystals in the control cold flow wax liberation needs to be better understood. The impact of potential nucleation of more stable wax in an annulus heating configuration is much in doubt and more validation is needful.

9. References

1. Aiyejina, A., et al., *Wax formation in oil pipelines: A critical review*. International Journal of Multiphase Flow, 2011. **37**(7): p. 671-694.
2. Valinejad, R. and A.R. Solaimany Nazar, *An experimental design approach for investigating the effects of operating factors on the wax deposition in pipelines*. Fuel, 2013. **106**(0): p. 843-850.
3. Huang, Z., et al., *The Effect of Operating Temperatures on Wax Deposition*. Energy & Fuels, 2011. **25**(11): p. 5180-5188.
4. Elsharkawy, A.M., T.A. Al-Sahhaf, and M.A. Fahim, *Wax deposition from Middle East crudes*. Fuel, 2000. **79**(9): p. 1047-1055.
5. Guozhong, Z. and L. Gang, *Study on the wax deposition of waxy crude in pipelines and its application*. Journal of Petroleum Science and Engineering, 2010. **70**(1–2): p. 1-9.
6. Granherne. *Wax Management*. 2008 [cited 2012 October 02]; Available from: http://www.surestream-fas.com/pdf/granherne/Wax_Jul_07_.pdf.
7. Ajayi, E.O., *Evaluation of methods of controlled wax deposition and loosening for oil and gas production*, 2013, Norwegian University of Science and Technology: Trondheim, Norway.
8. Lira-Galeana, C., A. Firoozabadi, and J.M. Prausnitz, *Thermodynamics of wax precipitation in petroleum mixtures*. AIChE Journal, 1996. **42**(1): p. 239-248.
9. Coutinho, J.A.P., et al., *Reliable Wax Predictions for Flow Assurance*. Energy & Fuels, 2006. **20**(3): p. 1081-1088.
10. Schou, P.K. and P.L. Christensen, *Phase Behavior of Petroleum Reservoir Fluids* 2007.
11. Rosvold, K., *Wax deposition models*, 2008, Norwegian University of Science and Technology NTNU: Trondheim, Norway.
12. International, A., *Standard test method for cloud point of petroleum mixture* 2011, ASTM International: United States.
13. International, A., *Standard Test Method for Cloud Point of Petroleum Products (Constant Cooling Rate Method)*, 2010, ASTM International: United States.
14. Hoffmann, R. and L. Amundsen, *Single-Phase Wax Deposition Experiments*. Energy & Fuels, 2010. **24**(2): p. 1069-1080.
15. Labes-Carrier, C., et al., *Wax Deposition in North Sea Gas Condensate and Oil Systems: Comparison Between Operational Experience and Model Prediction*, in *SPE Annual Technical Conference and Exhibition* 2002, Copyright 2002, Society of Petroleum Engineers Inc.: San Antonio, Texas.
16. Coto, B., et al., *A New DSC-Based Method to Determine the Wax Porosity of Mixtures Precipitated from Crude Oils*. Energy & Fuels, 2011. **25**(4): p. 1707-1713.

17. Brevik, J., *Wax control in production systems*, 2013, Statoil.
18. BASS, R.M. and C.G. LANGNER, *DIRECT ELECTRIC PIPELINE HEATING*, U.S.P.a.T. Office, Editor 2000, SHELL OIL COMPANY P.O. BOX 2463 900 LOUISIANA HOUSTON, TEXAS 77252-2463: USA.
19. Hoffman, R. and L. Amundsen, *METHOD FOR WAX REMOVAL AND MEASUREMENT OF WAX THICKNESS*, U.S.P.a.T. Office, Editor 2010, STATOIL ASA Stavanger NO: Norway.
20. Nexams, *Underwater hybrid cables Electrical Heating of Submarine flowlines (DEH)*, 2012.
21. Radan, D. *Power supply for (DEH) direct electric heating of long step out subsea pipelines*.
22. Milind Deo, J.M.a.R.R., *RPSEA 1201 Controlling Wax Deposition in the Presence of Hydrates Technology Evaluation Report*, 2010, University of Utah, Salt Lake City, UT 84112.
23. Edmonds, B., et al., *Simulating Wax Deposition in Pipelines for Flow Assurance*. Energy & Fuels, 2007. **22**(2): p. 729-741.
24. Pan, S., et al., *Case Studies on Simulation of Wax Deposition in Pipelines*, in *International Petroleum Technology Conference 2009*, 2009, International Petroleum Technology Conference: Doha, Qatar.
25. Burger, E.D., T.K. Perkins, and J.H. Striegler, *Studies of Wax Deposition in the Trans Alaska Pipeline*. SPE Journal of Petroleum Technology, 1981. **33**(6): p. 1075-1086.
26. Azevedo, L.F.A. and A.M. Teixeira, *A Critical Review of the Modeling of Wax Deposition Mechanisms*. Petroleum Science and Technology, 2003. **21**(3-4): p. 393-408.
27. Sarica Cem, V.M., *Tulsa University Paraffin Deposition Projects*, 2004, The University of Tulsa 600 South College Avenue Tulsa, Oklahoma 74104.
28. Calsep, *PVTsim 20 Method Documentation*
29. GROUP, S., *Wax- Methods and assumptins*, in *OLGA 7.1 user Manual* 2012.
30. Singh, P., et al., *Formation and aging of incipient thin film wax-oil gels*. AIChE Journal, 2000. **46**(5): p. 1059-1074.
31. Singh, P., et al., *Morphological evolution of thick wax deposits during aging*. AIChE Journal, 2001. **47**(1): p. 6-18.
32. Singh, A., et al., *Flow Assurance: Validation of Wax Deposition Models Using Field Data from a Subsea Pipeline*, in *Offshore Technology Conference 2011*: Houston, Texas USA.
33. Coutinho, J.A.P., J. Pauly, and J.-L. Daridon, *Chapter 10: Modelling phase equilibria in systems with organic solid solutions*, in *Computer Aided Chemical Engineering*, M.K. Georgios and G. Rafiqul, Editors. 2004, Elsevier. p. 229-249.
34. Schou Pedersen, K., P. Skovborg, and H.P. Roenningsen, *Wax precipitation from North Sea crude oils. 4. Thermodynamic modeling*. Energy & Fuels, 1991. **5**(6): p. 924-932.

35. Won, K.W., *Thermodynamic calculation of cloud point temperatures and wax phase compositions of refined hydrocarbon mixtures*. Fluid Phase Equilibria, 1989. **53**(0): p. 377-396.
36. Hansen, J.H., et al., *A thermodynamic model for predicting wax formation in crude oils*. AIChE Journal, 1988. **34**(12): p. 1937-1942.
37. Vafaie-Sefti, M., S.A. Mousavi-Dehghani, and M. Mohammad-Zadeh Bahar, *Modification of multisolid phase model for prediction of wax precipitation: a new and effective solution method*. Fluid Phase Equilibria, 2000. **173**(1): p. 65-80.
38. Twu, C.H., *An internally consistent correlation for predicting the critical properties and molecular weights of petroleum and coal-tar liquids*. Fluid Phase Equilibria, 1984. **16**(2): p. 137-150.
39. Coutinho, J.A.P., *Predictive UNIQUAC: A New Model for the Description of Multiphase Solid-Liquid Equilibria in Complex Hydrocarbon Mixtures*. Industrial & Engineering Chemistry Research, 1998. **37**(12): p. 4870-4875.
40. Bendiksen, K.H., et al., *The Dynamic Two-Fluid Model OLGA: Theory and Application*. SPE Production Engineering, 1991. **6**(2): p. 171-180.
41. Merino-Garcia, D. and S. Corraera, *Cold Flow: A Review of a Technology to Avoid Wax Deposition*. Petroleum Science and Technology, 2008. **26**(4): p. 446-459.
42. <http://www.engineering.uiowa.edu/~me140/Lecture/fugacity.pdf>, *Intermediate Thermodynamics*, in *Fugacity*2013.

10. Appendix

10.1. Thermodynamics of phase fugacity and the free energy

The fugacity of an equilibrium component is defined as the effective pressure possessing the same equivalent pressure potential as a real gas defined using the Gibbs free energy equation in (10.1).

$$dG = RTd\ln f \quad (10.1)$$

Where G is the molar Gibbs free energy, R is the gas constant.

For simple compressible systems

$$dG = VdP - SdT \quad (10.2)$$

For isothermal systems, equation (10.2) is derived to obtain equation (10.3) where S is the entropy of the system.

$$(dG)_T = VdP \quad (10.3)$$

The pressure dependence of the fugacity is thus derived combining equation (10.1) and (10.3) such that

$$d\ln f = \frac{VdP}{RT} \quad (10.4)$$

Integrating between a pressure P and reference pressure P_{ref} , equation (10.5) is derived such that V is the molar volume and T the temperature in Kelvin.

$$\ln\left(\frac{f(P)}{f(P_{ref})}\right) = \int_{P_{ref}}^P \frac{V}{RT} dP \quad (10.5)$$

For multi-phases systems, the liquid fugacity is derived as equation (10.7) from (10.5)

$$\ln\left(\frac{f^L(P)}{f^L(P_{ref})}\right) = \frac{V^L(P - P_{ref})}{RT} \quad (10.6)$$

$$f^L(P) = f^L(P_{ref}) \exp\frac{V^L(P - P_{ref})}{RT} \quad (10.7)$$

Likewise for the solid-wax fugacity is given by equation (10.8).

$$f^W(P) = f^W(P_{ref}) \exp\frac{V^W(P - P_{ref})}{RT} \quad (10.8)$$

For Equation (10.7) and (10.8), it is to be noted that the molar volume is approximated constant over wide pressure variations, therefore essentially incompressible.[42]

At equilibrium

$$f_i^V = f_i^L \quad (10.9)$$

Such that the vapour and liquid are defined by equation (10.10) at pressure P.

$$f_i^V = x_i^V \phi_i^V P; \quad f_i^L = x_i^L \phi_i^L P \quad (10.10)$$

Where ϕ_i is the fugacity coefficient of component i , x_i in mole fraction of component i in the liquid or gas phase respectively.

Another definition of the liquid phase fugacity using the activity coefficient is employed in equation (10.11) such that the equilibrium ratio (K ratio) expressed as the ratio of the mole fraction of the vapour/gas phase to the mole fraction of the liquid phase as represented in equation (10.12) can be derived as a function of the fugacity coefficient of component i in the respective phases given by equation (10.13)[10].

$$f_i^L = x_i^L \gamma_i^L f_i^{oL} \quad (10.11)$$

$$K_i = \frac{x_i^V}{x_i^L} \quad (10.12)$$

$$K_i = \frac{x_i^V}{x_i^L} = \frac{\phi_i^L}{\phi_i^V} \quad (10.13)$$

10.2. Gibbs Free Energy of pure components

Phase transitions of pure components from the solid to the liquid state can be rightly explained using the Gibbs free energy theory.

$$dG = dH - TdS \quad (10.14)$$

$$dH = C_p dT \quad (10.15)$$

$$\Delta S = \frac{\Delta H}{T} \quad (10.16)$$

Where dG is the change in free energy, dH the enthalpy change, C_p is the heat capacity and dS is the entropy change at constant pressure respectively.

The free energy equation (10.14) determines the spontaneity of reactions such a negative dG indicates a spontaneous reaction – a spontaneous (melting) transition from the solid to the liquid phases. A positive dG indicates a solid-liquid system favourable to remain in the solid state. Zero dG value confirms a thermodynamically stable system such that both solid and liquid states are equally favourable and that the components are right at the melting points[10].

Applied to the fusion (melting) of component i , the free energy equation of fusion in equation (10.17) is obtained where subscript f represents the fusion component of component i , dH_i^f is the enthalpy of fusion and dS_i^f is the entropy of fusion of component i respectively.

$$\Delta G_i^f = \Delta H_i^f - T \Delta S_i^f \quad (10.17)$$

At melting temperature $dG = 0$, T_i^f is the melting temperature of component i , the entropy of fusion ΔS_i^f is also obtained as equation (10.18).

$$\Delta S_i^f = \frac{\Delta H_i^f}{T_i^f} \quad (10.18)$$

The free energy of fusion ΔG_i^f is giving as equation (10.19) assuming that the heat capacity term defined in equation (10.20) and (10.21) is zero.

$$\Delta G_i^f = \Delta H_i^f \left(1 - \frac{T}{T_i^f} \right) \quad (10.19)$$

The total enthalpy changes of component i from the solid to the liquid state is defined by equation (10.20). Likewise the total entropy change of phase transition from the solid to the liquid state is derived as equation (10.21) such that $T \neq T_i^f$, ΔC_{p_i} is the heat capacity difference between the solid and liquid state heat capacities of component i ,

$$\Delta H = \Delta H_i^f + \int_T^{T_i^f} \Delta C_{p_i} dT \quad (10.20)$$

$$\Delta S = \frac{\Delta H_i^f}{T_i^f} + \int_T^{T_i^f} \frac{\Delta C_{p_i}}{T} dT \quad (10.21)$$

The Gibbs free energy relation of component i with the fugacity of component i as defined in equation (10.1) is given in equation (10.22).

$$dG_i = RT d \ln f_i \quad (10.22)$$

The referenced fugacity of pure component undergoing phase transition at referenced atmospheric pressure P_{ref} such that ΔH_i^f , and T_i^f are measured at the reference pressure P_{ref} is obtained in equation (10.23).

$$\Delta G = RT \ln \left(\frac{f_i^{oL}(\mathbf{P}_{ref})}{f_i^{oW}(\mathbf{P}_{ref})} \right) = RT \left(\ln f_i^{oL}(\mathbf{P}_{ref}) - f_i^{oW}(\mathbf{P}_{ref}) \right) \quad (10.23)$$

Putting equation (10.20), (10.21) and (10.23) in equation (10.14), equation (10.24) is obtained for pure solid fugacity at reference pressure \mathbf{P}_{ref} .

$$f_i^{oW}(\mathbf{P}_{ref}) = f_i^{oL}(\mathbf{P}_{ref}) \exp \left(-\frac{\Delta H_i^f}{RT} \left[1 - \frac{T}{T_i^f} \right] - \frac{1}{RT} \int_T^{T_i^f} \Delta C_{P_i} dT + \frac{1}{RT} \int_T^{T_i^f} \frac{\Delta C_{P_i}}{T} dT \right) \quad (10.24)$$

Combining the pressure dependence of the fugacity of equation (10.7) and (10.8) for the liquid and wax phase respectively we have the fugacity of pure wax of component i at pressure P calculated by equation (10.25). Where ΔV_i is the difference in molar volume of component i .

$$f_i^{oW}(P) = f_i^{oL}(P) \exp \left(-\frac{\Delta H_i^f}{RT} \left[1 - \frac{T}{T_i^f} \right] - \frac{1}{RT} \int_T^{T_i^f} \Delta C_{P_i} dT + \frac{1}{RT} \int_T^{T_i^f} \frac{\Delta C_{P_i}}{T} dT + \frac{\Delta V_i(P - P_{ref})}{RT} \right) \quad (10.25)$$

10.3. SRK expression of the fugacity coefficient

$$\ln \phi = -\ln(Z - B) + (Z - 1) \frac{b_i}{b} - \frac{A}{B} \left[\frac{1}{a} \left(2\sqrt{a_i} \sum_{j=1}^N z_j \sqrt{a_j} (1 - k_{ij}) \right) - \frac{b_i}{b} \right] \ln \left(1 + \frac{B}{Z} \right) \quad (10.26)$$

$$Z = \frac{PV}{RT} \quad (10.27)$$

$$A = \frac{a(T)P}{R^2T^2} \quad (10.28)$$

$$B = \frac{bP}{RT} \quad (10.29)$$

$$a = \sum_{i=1}^N \sum_{j=1}^N z_i z_j a_{ij} \quad (10.30)$$

$$b = \sum_{i=1}^N z_i b_i \quad (10.31)$$

$$a_{ij} = \sqrt{a_i a_j} (1 - k_{ij}) \quad (10.32)$$

Where k_{ij} is a binary interaction parameter, z is the mole fraction for component indices i and j , a and b are mixture components and Z is the compressibility factor.

10.4. Plots of wax deposition models in OLGA

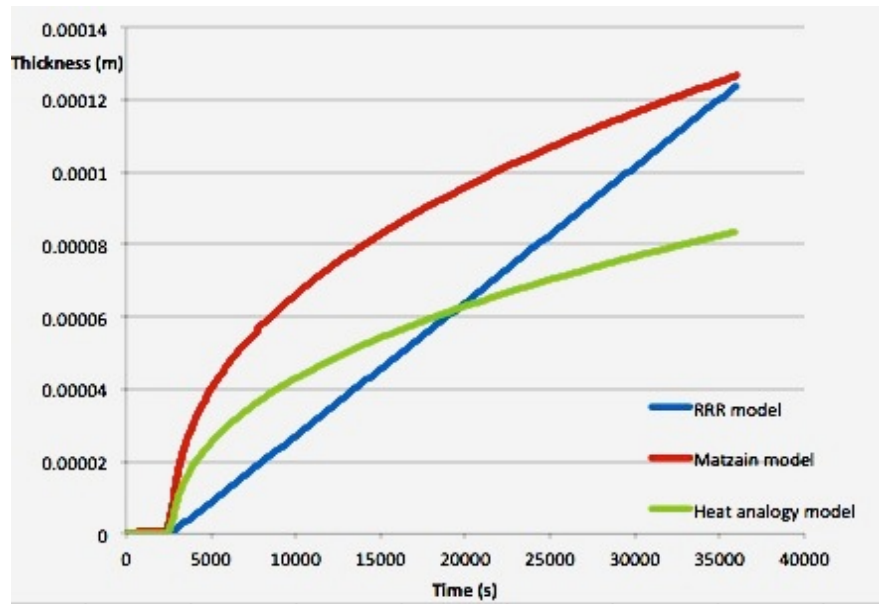


Figure 10-1 Trend plot of wax thickness in pipe 2 for RRR, Matzain and Heat Analogy model[7]